PLOS ONE

RESEARCH ARTICLE

Amnion-Epithelial-Cell-Derived Exosomes Demonstrate Physiologic State of Cell under Oxidative Stress

Samantha Sheller[1,2], John Papaconstantinou[2], Rheanna Urrabaz-Garza[1], Lauren Richardson[1], George Saade[1], Carlos Salomon[3], Ramkumar Menon[1]*

1 Division of Maternal-Fetal Medicine & Perinatal Research, Department of Obstetrics & Gynecology, The University of Texas Medical Branch at Galveston, Galveston, Texas, United States of America, **2** Department of Biochemistry and Molecular Biology, The University of Texas Medical Branch at Galveston, Galveston, Texas, United States of America, **3** Exosome Biology Laboratory, Centre for Clinical Diagnostics, UQ Centre for Clinical Research, Faculty of Health Sciences, University of Queensland, Herston, Queensland, Australia

* ram.menon@utmb.edu

OPEN ACCESS

Citation: Sheller S, Papaconstantinou J, Urrabaz-Garza R, Richardson L, Saade G, Salomon C, et al. (2016) Amnion-Epithelial-Cell-Derived Exosomes Demonstrate Physiologic State of Cell under Oxidative Stress. PLoS ONE 11(6): e0157614. doi:10.1371/journal.pone.0157614

Editor: Kang Sun, Shanghai Jiaotong University School of Medicine, CHINA

Received: April 14, 2016

Accepted: June 1, 2016

Published: June 22, 2016

Data Availability Statement: All relevant data are within the paper and its Supporting Information files.

Funding: This study is supported by Innovative catalyst grant funding from March of Dimes Center of Ohio, Cincinnati, OH to RM and partially by RM's Faculty development funds from University of Texas Medical Branch at Galveston, TX. Authors declare *all* the funding or sources of support received during this specific study. The funders had no role in study design, data collection and analysis, decision to publish, or preparation of the manuscript.

Abstract

At term, the signals of fetal maturity and feto-placental tissue aging prompt uterine readiness for delivery by transitioning quiescent myometrium to an active stage. It is still unclear how the signals reach the distant myometrium. Exosomes are a specific type of extracellular vesicle (EVs) that transport molecular signals between cells, and are released from a wide range of cells, including the maternal and fetal cells. In this study, we hypothesize that *i*) exosomes act as carriers of signals in utero-placental compartments and *ii*) exosomes reflect the physiologic status of the origin cells. The primary aims of this study were to determine exosomal contents in exosomes derived from primary amnion epithelial cells (AEC). We also determined the effect of oxidative stress on AEC derived exosomal cargo contents. AEC were isolated from amniotic membrane obtained from normal, term, not in labor placentae at delivery, and culture under standard conditions. Oxidative stress was induced using cigarette smoke extract for 48 hours. AEC-conditioned media were collected and exosomes isolated by differential centrifugations. Both growth conditions (normal and oxidative stress induced) produced cup shaped exosomes of around 50 nm, expressed exosomes enriched markers, such as CD9, CD63, CD81 and HSC70, embryonic stem cell marker Nanog, and contained similar amounts of cell free AEC DNA. Using confocal microscopy, the colocalization of histone (H) 3, heat shock protein (HSP) 70 and activated form of pro-senescence and term parturition associated marker p38 mitogen activated protein kinase (MAPK) (P-p38 MAPK) co-localized with exosome enrich marker CD9. HSP70 and P-p38 MAPK were significantly higher in exosomes from AEC grown under oxidative stress conditions than standard conditions ($p<0.05$). Finally, mass spectrometry and bioinformatics analysis identified 221 different proteins involved in immunomodulatory response and cell-to-cell communication. This study determined AEC exosome characteristics and their cargo reflected the physiologic status of the cell of origin and suggests that AEC-derived exosomal p38 MAPK plays a major role in determining the fate of pregnancy. Understanding the

Competing Interests: The authors have declared that no competing interests exist.

propagation of fetal signals and their mechanisms in normal term pregnancies can provide insights into pathologic activation of such signals associated with spontaneous preterm parturitions.

Introduction

Normal term human parturition is initiated between 37 and 40 weeks of gestation when in utero fetal growth and development are completed [1–3]. The signals from mature fetal organs prompt uterine readiness for delivery by transitioning quiescent myometrium to an active stage (contractile phenotype) [2,4,5]. Various endocrine, immune and mechanical signals from feto-maternal compartments enhance overall uterine inflammatory load leading to functional progesterone withdrawal causing myometrial contractility [6–8]. Therefore, term labor and delivery results from well-orchestrated activities of various endocrine and paracrine factors. Nonetheless, the signature of these signals and their precise mechanisms in initiating parturition are still unclear and under investigation by many laboratories. Understanding the mechanisms of these signals in normal term pregnancies can provide insights into pathologic activation that can cause spontaneous preterm parturitions.

Recently, our laboratory has reported fetal membrane (amniochorionic membrane) senescence as a mechanism associated with normal term parturition [9,10]. Placental membranes undergo an oxidative stress associated telomere dependent cellular senescence at term [11–13]. In addition, placental membrane senescence is also associated with sterile inflammation in the amniotic fluid [9,14]The unique inflammation seen in senescent cells is defined senescence associated secretory phenotype (SASP) [15]. SASP is characterized by proinflammatory cytokines and chemokines that are reported to be associated with term labor and delivery [9]. The findings in clinical specimens have been reproduced in vitro in primary amnion epithelial cells in culture exposed to oxidative stress induced by cigarette smoke extract (CSE) [12]. Generation of senescence and SASP were reduced by inhibiting p38 mitogen activated kinase (MAPK), a stress associated pro-senescence protein, suggesting that sterile inflammation can be generated by senescent cells [12,14,16].

It is still unclear how proinflammatory SASP signals from senescent fetal membranes can reach distant myometrium or whether they are confined to enforcing local (fetal) tissue damage and inflammation until parturition. Senescent signals may be transported to distant tissues indicating a dysfunctional fetal membrane status that prompts delivery of the fetus, as well as placenta and membrane. Although localized activities of SASP can be achieved through direct cell-cell contact or through ligand-receptor interactions, distant feto-maternal communication is likely facilitated through specific carriers that can transport and deliver signals from senescent cells. Thus, prior to projecting senescent fetal cells signaling parturition at a distant myometrium, the mode of delivery of such signals must be established. Several recent reports and reviews propose a role for exosomes as such carriers of parturition signals to utero-placental compartments [17–20].

Exosomes are 30–100 nm endosome-derived vesicles with specific characteristics that separate them from other larger particles such as microvesicles and apoptotic bodies [21–24]. Exosome biogenesis is a process that begins with the endocytosis of transmembrane proteins [25,26]. Once sorted to late endosomes, the endosomal sorting complex required for transport (ESCRT) complex, recruits proteins and other cargo, while also mediating the inward budding of the late endosome, creating the intraluminal vesicles inside the multivesicular body (MVB) [27–30]. The MVB can either follow a degradation pathway fusing with lysosomes or proceed

to release the intraluminal vesicles into the extracellular space through exocytosis as exosomes [27,28]. Placental derived exosomes have been well characterized during normal and abnormal pregnancies and their functional roles have also been documented [4–13,31–39]. Their size facilitates easy transportation between cells and tissues, while their contents reflect the state of the source cell and regulate the phenotype of the target cell [23,34,36,40–42]. Exosomes interact with the target cell by direct fusion with the cell membrane, thus releasing the contents directly into the cytosol; through active uptake via endocytosis or by binding to the target cell via receptor-ligand interactions thereby inducing a signaling cascade which changes the phenotype of the target cell.

No reports exist on fetal membrane- derived exosomes or their contents. Therefore, the objectives of this study are: 1) determine the generation of exosomes from primary amnion epithelial cells and characterize their contents, 2) determine the changes in specific exosome contents in primary amnion cells in response to oxidative stress. Since p38 MAPK was identified as a crucial stress response-signaling pathway that activates oxidative stress induced senescence at term, we specifically examined exosomal p38 MAPK cargo. Using an in vitro primary amnion epithelial cell (AEC) model of oxidative stress induced by cigarette smoke extract, a well characterized model of in vitro oxidative stress, and using Liquid Chromatography (LC)/ Mass Spectrometry (MS) we characterize the contents of AEC -derived exosomes and their potential role in parturition.

Materials and Methods

Placental samples were obtained for this study from John Sealy Hospital at The University of Texas Medical Branch (UTMB) at Galveston, TX, USA. No subjects were recruited or consented for this study as we used discarded placenta from normal term, not in labor cesarean sections. The study protocol was submitted and approved by the institutional review board at UTMB, whereby placental samples could be collected without consenting subjects. Placentae from women (18–40 years old) undergoing elective repeat cesarean delivery (between 37 and 41 weeks of gestation) prior to the onset of labor were included in the study. Women with prior history of preterm labor and delivery, preterm premature rupture of the membranes, preeclampsia, placental abruption, intrauterine growth restriction, and gestational diabetes were excluded. Additionally, group B *streptococcus* carriers, treated for urinary tract infection, sexually transmitted diseases, chronic infections like HIV, hepatitis, and women who smoked cigarettes or reported drug and alcohol abuse, were also excluded.

Isolation and Culture of human Amnion Epithelial Cells (AECs)

All reagents and media were warmed to 37°C prior to use. The amniotic membrane was processed as described previously [6, 12, 14] Briefly, the amnion membrane was manually peeled from normal, term, not in labor caesarean section placentas, rinsed in saline and transferred to a petri dish containing Hanks Balanced Salt Solution (HBSS; Mediatech Inc., Manassas, VA). After cutting the amnion into 2 cm x 2 cm pieces, they were digested twice in 0.25% trypsin and 0.125% Collagenase A (Sigma–Aldrich, St. Louis, MO) in HBSS for 35 minutes at 37°C. After each digestion, the tissue was filtered through a 70 μm cell strainer (Thermo Fisher Scientific, Waltham, MA) and trypsin was inactivated using complete Dulbecco's Modified Eagle Medium: Nutrient Mixture F-12 media (DMEM/F12; Mediatech Inc.) supplemented with 15% fetal bovine serum (FBS; Sigma-Aldrich), 10% Penicillin/Streptomycin (Mediatech Inc.) and 100 μg/mL epidermal growth factor (EGF; Sigma-Aldrich). The collected filtrate was centrifuged for 10 minutes at 3000 RPM and the pellet was resuspended in 3.0 mL complete DMEM/F12. Once cells were counted, approximately 3–5 million cells per flask were cultured in T75

flasks containing complete DMEM/F12 media at 37°C, 5% CO_2, and 95% air humidity to 70–80% confluence.

To ensure the purity of our primary AEC cultures, immunofluorescent staining was performed. Cells were seeded on glass coverslips at a density of 30,000 cells per slip and incubated overnight. Cells were fixed with 4% paraformaldehyde (PFA), permeablized with 0.5% Triton X and blocked with 3% BSA in PBS prior to incubation with Cytokeratin 18 (Abcam, Cambridge, United Kingdom) primary antibody diluted 1:300 in 3% BSA overnight at 4°C. After washing with PBS, slides were incubated Alexa Fluor conjugated secondary antibodies (Life Technologies, Carlsbad, CA) diluted 1:400 in PBS for 1 hour in the dark. Slides were washed with PBS then treated with NucBlue® Live ReadyProbes® Reagent (Life Technologies) then mounted using Mowiol 4–88 mounting medium (Sigma-Aldrich). Images were captured using LSM 510 Meta UV confocal microscope (63x) (Zeiss, Germany).

Stimulation of AEC with cigarette smoke extract (CSE)

To induce oxidative stress in AECs, CSE was used as detailed in our prior studies, [12,43,44] with modifications. Smoke from a single lit commercial cigarette (unfiltered Camel™, R.J. Reynolds Tobacco Co, Winston Salem, NC) was infused into 25 mL of exosome-free media, consisting of DMEM/F12 supplemented with 10% exosome-free FBS (System Biosciences, Mountain View, CA). The stock CSE was sterilized using 0.25 mm Steriflip® filter unit (Millipore, Billerica, MA). CSE concentrate was diluted 1:10 in exosome-free media prior to use. Once cells reached 70–80% confluence, each flask was rinsed with sterile 1x PBS followed by treatment with exosome-free media (control) or CSE containing media and incubated at 37°C, 5% CO_2, and 95% air humidity for 48 hours.

Cell cycle analysis of AECs using flow cytometry

CSE treated and control AECs were harvested after media collection using trypsin EDTA (Corning, Corning, NY) and centrifuged for 10 minutes at 3000 RPM. The supernatant was removed and cells were resuspended in 50 μL PBS. Cell cycle analysis was performed using the Coulter DNA Prep Reagents Kit (Beckman Coulter, Indianapolis, IN). Briefly, 50 μL of DNA Prep LPR was added to each sample and vortexed. Then 1.0 mL DNA Prep Stain was added to the tubes, vortexed and run immediately on the Cytoflex flow cytometer (Beckman Coulter). After selecting for single cells, gating was set for the control cells and applied to histograms for the CSE treated AECs using Cytexpert (Beckman Coulter).

Activation of p38 MAPK in AECs using flow cytometry

Activation of p38 MAPK was also performed. After harvesting cells using trypsin EDTA and centrifugation for 10 minutes at 3000 RPM, the pellet was resuspended in 500 μL 4% paraformaldehyde and vortexed. After incubation for 10 minutes at room temperature, cells were placed on ice for 1 minute then centrifuged for 5 minutes at 2000 RPM at 4°C. The supernatant was removed and the pellet was resuspended in 500 μL 90% ice cold methanol, gently vortexing while adding methanol slowly. Once the pellet was completely resuspended, the cells were incubated on ice for 10 minutes then stored at -20°C until use.

All centrifugations were performed at 2000 RPM for 5 minutes at 4°C. Cells in 90% methanol were centrifuged and washed twice with 5% BSA in PBS. After the second centrifugation, the pellet was resuspended in P-p38 MAPK primary antibody (Cell Signaling) diluted 1:200 in 5% BSA and incubated at room temperature for 2 hours. Cells were washed twice with 5% BSA in PBS then resuspended in Alexa Fluor conjugated secondary antibody (Life Technologies) diluted 1:400 in PBS and incubated for 1 hour at room temperature in the dark. Cells were

centrifuged and resuspended in 400 μL PBS and run immediately on the Cytoflex flow cytometer (Beckman Coulter). After gating for single cells, data analysis based was performed using Cytexpert (Beckman Coulter). Flow Cytometry analysis for exosome markers and DNA

Exosome isolation

The culture media were collected and stored at -80°C until exosome isolation. Media was thawed overnight then isolated using differential ultracentrifugation as described previously, with modifications [21,45,46]. Briefly, the culture media was centrifuged sequentially at 4°C for 10 minutes at 300g and 20 minutes at 2,000g using Sorvall Legend X1R and TX-400 swinging bucket rotor (Thermo Fisher Scientific), 30 minutes at 10,000g and 2 hours at 100,000g using a Beckman Optima LX-80 ultracentrifuge with 50.1Ti and 70.1Ti rotors (Beckman Coulter). The pellet was resuspended in 1x PBS then centrifuged again at 100,000g for 1 hour. Pellet was resuspended in RIPA (Western Blot) or 1x PBS (electron microscopy, Flow Cytometry, DNA quant and sizing).

Transmission Electron Microscopy (TEM) of whole mounted exosomes

For TEM studies, 5 μL suspended exosomes in PBS were dropped onto a formvar-carbon coated 300-mesh copper grid and left to dry at room temperature for 10 min. Grids were treated with 10 seconds of Hydrogen-Oxygen plasma in a Gatan Solarus 950 plasma cleaning system (Gatan, Inc., Pleasanton, CA) prior to use. After three washes in purified water, the exosome samples were negatively stained using PhosphoTungstic Acid (PTA). The grids were dried at room temperature then viewed in a 120 keV JEM 1400 electron microscope (Jeol, Peabody, MA). A minimum of 10 frames were viewed per sample.

Exosome particle sizing analysis

Dynamic light scattering analysis (DLS) was used to determine the mean size distribution and purity of our exosome preps. 50 μL of concentrated exosomes was brought to a volume of 1.0 mL in 1x PBS and sized using Malvern High Performance Particle Sizer (HPPS) (Malvern Instruments, Worcestershire, UK).

Western blot analysis

Exosomal pellets were resuspended in RIPA lysis buffer (50 mM Tris pH 8.0, 150 mM NaCl, 1% Triton X-100, and 1.0 mM EDTA pH 8.0, 0.1% SDS) supplemented with protease and phosphatase inhibitor cocktail and PMSF. After centrifugation at 10,000 RPM for 20 minutes, the supernatant was collected and protein concentrations were determined using BCA (Pierce, Rockford, IL). The protein samples were separated using SDS-PAGE on a gradient (4–15%) Mini-PROTEAN® TGX™ Precast Gels (Bio-Rad, Hercules, CA) and transferred to the membrane using iBlot® Gel Transfer Device (Thermo Fisher Scientific). Membranes were blocked in 5% nonfat milk in 1x Tris buffered saline-Tween 20 (TBS-T) buffer for a minimum of 1 h at room temperature then probed (or re-probed) with primary antibody overnight at 4°C. The membrane was incubated with suitable secondary antibody conjugated with horseradish peroxidase and immunoreactive proteins were visualized using Luminata Forte Western HRP substrate (Millipore, Billerica, MA). The stripping protocol followed the instructions of Restore Western Blot Stripping Buffer (Thermo Fisher). No blots were used more than three times.

The following anti-human antibodies were used for western blot: Exosome markers CD81 (Abnova, Taiwan) and heat shock cognate (HSC) 70 (Abcam) were diluted 1:500, while ESCRT complex protein Alix (Santa Cruz Biotechnology, Dallas, TX) was diluted 1:200.

Embryonic stem cell markers Nanog andOCT-4, (Cell Signaling, Beverly, MA) were diluted 1:500. Heat shock protein (HSP) 70 (Abcam), a damage associated molecular pattern, was diluted 1:500. Total p38 MAPK and phospho p38 MAPK (Cell Signaling) were diluted 1:400.

Flow Cytometry analysis for exosome markers and DNA

For flow cytometry analysis of exosome tetraspanin markers CD9, CD63 and CD81, a total of five samples per condition were prepared using the ExoFlow kit (System Biosciences) protocol with modifications. Briefly, exosomes isolated from treated and untreated amnion cell cultures were resuspended in 150 μL 1x PBS and all kit reagent volumes were halved. Streptavidin coated 9.1μm beads were washed then incubated with biotinylated anti-CD9, CD63 or CD81 for 2 hours on ice, flicking intermittently to mix. Beads were washed and resuspended in 200 μL bead wash buffer prior to incubation overnight at 4°C with 50 μL exosomes (total volume 250 μL). The following day, samples were washed and stained using the Exo-FITC exosome stain according to manufacturer then run on the Cytoflex flow cytometer (Beckman Coulter). Negative controls with isotype-matched antibodies were used for gating, applied according to manufacturer instructions. Data analysis based on fluorescein isothiocyanate (FITC) signal shift was performed using Cytexpert (Beckman Coulter).

After initial analysis for tetraspanin markers, the samples were tested for DNA content using the Coulter DNA Prep Reagents Kit (Beckman Coulter), which uses propidium iodide to tag DNA. Since DNA fragments are expected to stick to exosomal membranes and can confound with true exosomal DNA cargo, AEC exosomes were pretreated with DNase to remove all external DNA. To address the potential contamination, the samples were split in half, one set of samples were pretreated with DNase while the other half remained untreated. Pretreated samples were washed with exosome wash buffer provided in the ExoFlow kit then resuspended in DNase 1 set (Zymo Research, Irvine, CA) solution according to the manufacturer's protocol, substituting exosome wash buffer for ethanol. Samples were incubated at room temperature for 10 minutes. To inactivate the DNase, samples were heated to 65°C for 15 minutes. After washing with exosome wash buffer three times, the pretreated and untreated exosomes were resuspended in 50 μL PBS then stained using the Coulter DNA Prep kit (Beckman Coulter). Samples were run on the Beckman Coulter CytoFlex Flow Cytometer. Negative controls, consisting of beads without exosomes attached, were used for gating, applied according to ExoFlow (SBI) instructions.

Quantitation of exosomal DNA

To quantify the amount of DNA, exosomes were resuspended in 200 μL 1x PBS. DNA was extracted following DNeasy Blood and Tissue kit protocol (Qiagen, Hilden, Germany). Quantification was performed on the Synergy H4 Hybrid Microplate Reader (Biotek, Winooski, VT) using the Take 3 microvolume plate and Gen5 software (Biotek). We corrected for the blank and DNA concentration was calculated based on the absorbance ratio of 280/260.

Immunofluorescence staining and microscopy

Cells were seeded on glass coverslips at a density of 30,000 cells per slip and incubated overnight prior to treatment with either exosome-free media (control) or 1:10 dilution of fresh CSE in exosome-free media. After 24 hour treatment, cells were fixed with 4% paraformaldehyde (PFA), permeablized with 0.5% Triton X and blocked with 3% BSA in PBS prior to incubation with primary antibodies overnight at 4°C. After washing with PBS, slides were incubated Alexa Fluor 488– or 594–conjugated secondary antibodies (Life Technologies) diluted 1:400 in PBS for 1 hour in the dark. Slides were washed with PBS then treated with NucBlue® Live ReadyProbes® Reagent (Life Technologies) then mounted using Mowiol 4–88 mounting medium

(Sigma-Aldrich). Images were captured using LSM 510 Meta UV confocal microscope (63x) (Zeiss, Germany). Exosomes were tagged using anti-CD9 diluted 1:300, while P-p38 MAPK, Histone 3 (H3), and HSP70 were diluted 1:250. Colocalization of proteins of interest with exosomes was determined using LSM software (Zeiss) and Image J (open source). A total of five images per condition and 5 regions of interest per image were used to determine red and green fluorescence intensity values per distance (μm). Intensity was graphed versus distance for both colors using GraphPad Prism (GraphPad Software, La Jolla, CA). Areas of overlap indicate colocalization. The images were also analyzed for Pearson's Correlation Coefficient using Coloc 2 from Fiji (open source), selecting 5 regions of interest for each image. Mean Pearson's values were graphed using Excel. Any image modifications (brightness, contrast, and smoothing) were applied to the entire image using Image J (open source).

Proteomic analysis of AEC-derived exosomes by mass spectrometry

Protein profile of exosomes isolated from AEC culture under normal or oxidative stress conditions were established by Liquid Chromatography (LC)/ Mass Spectrometry (MS) as previously described with modifications [41,42]. Briefly, exosome pellets were lysed in 500μL modified RIPA buffer (2.0% SDS, 150mM NaCl, 50mM Tris, pH 8.5, 1X Complete Protease inhibitor (Roche)) at 100°C for 15 minutes. The lysate was clarified by centrifugation and the protein concentration determined by Qubit fluorometry (Invitrogen). 10 μg of extracted protein was processed by SDS-PAGE using 10% Bis Tris NuPage mini-gel (Invitrogen) in the MES buffer system. The migration window (2cm lane) was excised and in-gel digestion performed using a ProGest robot (DigiLab) using ammonium bicarbonate (25mM), dithiothreitol (reduction step, 10mM at 60°C) and iodoacetamide (alkylation step, 50mM). Samples were digested with sequencing grade trypsin (Promega) at 37°C for 4h and quenched with formic acid. The supernatant was analyzed directly without further processing. Digested samples were analyzed by nano LC-MS/MS with a Waters NanoAcquity HPLC system interfaced to a ThermoFisher Q Exactive. Peptides were loaded on a trapping column and eluted over a 75μm analytical column at 350nL/min using a 2hr reverse phase gradient; both columns were packed with Jupiter Proteo resin (Phenomenex). The mass spectrometer was operated in data-dependent mode, with the Orbitrap operating at 60,000 FWHM and 17,500 FWHM for MS and MS/MS respectively. The fifteen most abundant ions were selected for MS/MS. False discovery rate (FDR) was estimated using a reversed sequence database.

Functional analysis of exosome proteome

Proteins identified by MS/MS were analyzed by PANTHER (Protein Analysis THrough Evolutionary Relationships; http://www.pantherdb.org) as previously described [41,42]. Differentially identified proteins were analyzed further by bioinformatic pathway analysis (Ingenuity Pathway Analysis [IPA]; Ingenuity Systems, Mountain View, CA; www.ingenuity.com).

Statistical analysis

SPSS software (IBM, Armonk, NY) was used for statistical evaluation. Samples were analyzed using paired *t*–test and a *P* value less than 0.05 was considered statistically significant.

Results

Primary AEC cultures are positive for cytokeratin

Primary amnion cells isolated from term, not in labor C-sections were positive for cytokeratin 18, a commonly used marker for epithelial cells (Fig 1).

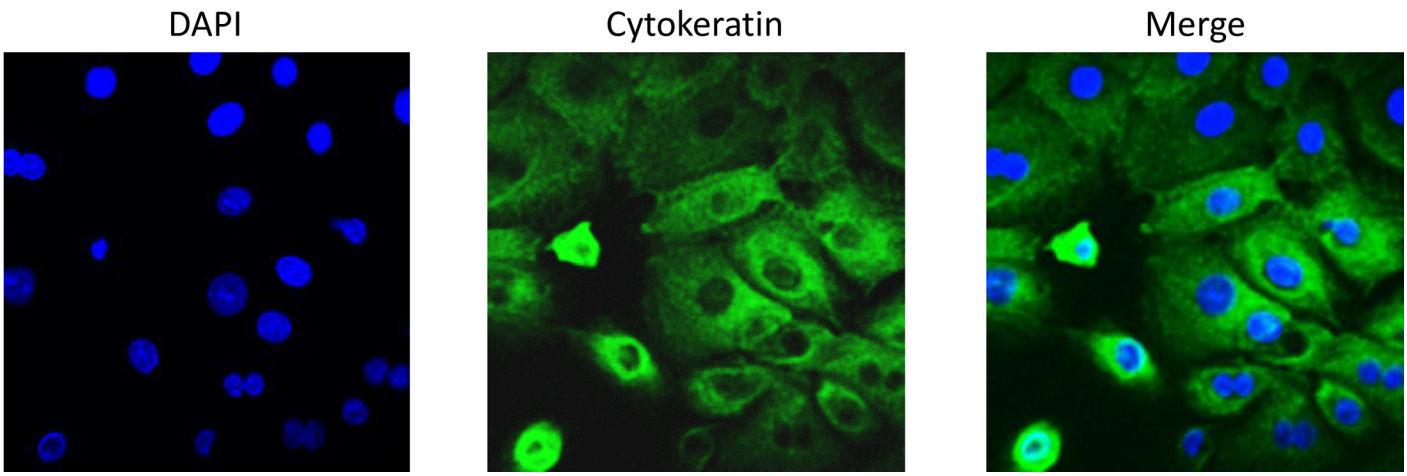

Fig 1. Cytokeratin staining of primary AECs. Primary AECs were fluorescently labeled for cytokeratin 18 to show cultures were predominantly epithelial cells. AEC-amnion epithelial cell.

doi:10.1371/journal.pone.0157614.g001

Cell cycle analysis and p38 MAPK activation of control and CSE treated AECs

To determine the pattern of the cell cycle in control and CSE AECs, cell cycle analysis was performed. Table 1 summarizes the results of the cell cycle analysis. While majority of the control and CSE treated AECs were in G1 phase, noticeable differences between the two groups can be seen (Table 1). As can be seen in Table 1, the percentage of SubG0G1 phase cells was much higher in CSE treated AECs than controls. The SubG0G1 phase includes cellular debris, as well as late apoptotic and necrotic cells and suggestive of cell cycle arrest and senescence associated changes after CSE treatment. The percentage of control cells in S phase and G2 (indicating active proliferation) were almost double in control compared to CSE treated AECs showing normal progression of cell cycles in these cells. These data represent the physiologic state of the cell.

To further confirm this physiologic state, we also examined p38MAPK activation, an oxidative stress response indicator activated by various stressors, using flow cytometry. AECs treated with CSE showed higher p38 MAPK activation than control cells, indicating CSE AECs were undergoing oxidative stress and cellular senescence.

Characteristics of exosomes released by primary amnion epithelial cells under control and CSE conditions

Exosomes isolated from AECs under standard (control) and oxidative (CSE) conditions were characterized using four different methods–electron microscopy (for shape and morphology), particle sizing (size), western blot and flow cytometry (specific markers and cargo contents) and Nano drop analysis (DNA quantitation).

Table 1. Cell cycle analysis and p38 MAPK activation of control and CSE treated amnion cells.

	SubG0G1	G1	S	G2	P-p38 MAPK
Control (untreated) AEC	**6.9%**	**73.4%**	**15.6%**	**4.1%**	**1.8%**
CSE Treated AEC	**36.4%**	**53.6%**	**7.9%**	**2.1%**	**35.9%**

doi:10.1371/journal.pone.0157614.t001

Exosome size and morphology from Control and CSE cells

TEM analysis (Fig 2A) revealed vesicles with classic exosomal morphology. Both untreated AECs and CSE treated AECs produced cup shaped vesicles with a size distribution between 30–50 nm, which is consistent with published reports for exosomes in general, as well for exosomes from reproductive tissues [31,34,47,48]. Size distribution by intensity graphs for control and CSE treated AEC exosomes indicate the absence of larger material in each sample (Fig 2B), such as microvesicles and apoptotic bodies validating our isolation procedures and purity of exosome preparations. DLS analysis also confirmed the size distribution of 3 control and 3 CSE exosome isolations (mean ±STD) (control 39.1±2.97; CSE 45.5±2.34). CSE treated AECs produced slightly larger exosomes than exosomes from untreated AECs ($p < 0.05$). The number of exosomes as determined by total protein concentrations per 1 million cells were similar under both conditions. However, we acknowledge that this is not the best approach to quantitate exosomes.

Exosome and AEC specific markers from Control and CSE cells

Western blot analysis was performed to determine exosome enriched markers and cargo contents. AEC exosomes showed the presence of markers CD81 and HSC70 (Fig 2C) regardless of

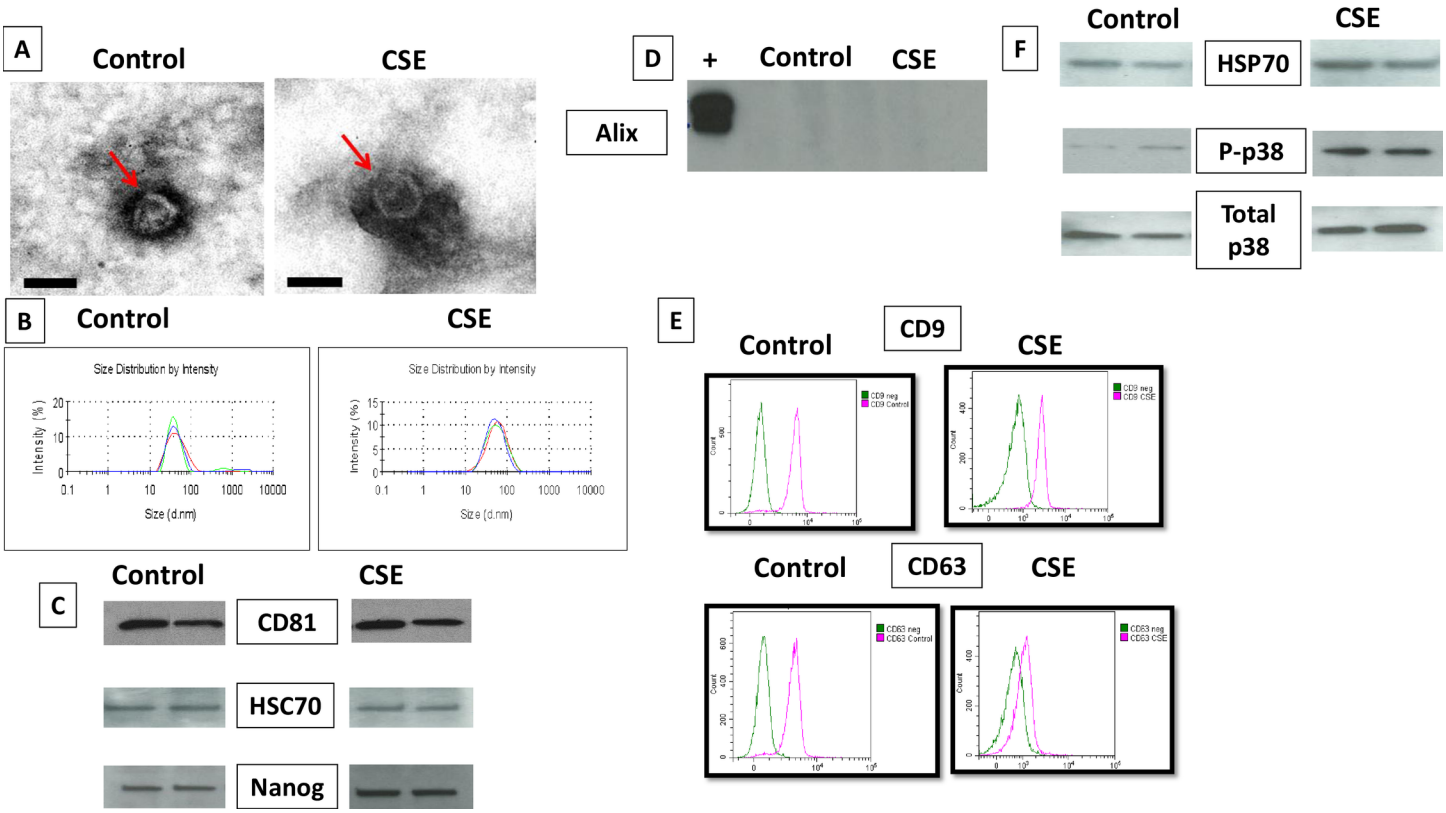

Fig 2. Characterization of exosomes released from amnion cells grown under standard (control) and oxidative (CSE) conditions. A: Electron microscopy showing cup-shaped vesicles that have a size distribution of 30–50 nm (arrow indicates exosomes, scale bar represents 50 nm). B: Size distribution analysis of exosomes from amnion cells untreated control (39.16 ±2.97) and CSE (45.53 ±2.34) exosomes. P<0.05 using paired sample t test. C: Western blot analysis showed the presence of exosome markers CD81 and HSC70, as well as embryonic stem cell marker, Nanog, indicating amnion epithelial cell origin. D: Western blot analysis shows lack of expression of Alix in AEC derived exosomes. E: Flow cytometric characterization of exosome tetraspanin markers exosome markers CD9 and CD63. X-axis is FITC intensity, y-axis is count, or number of beads positive for exosomes. Green represents negative control (neg). F: Western blot analysis showing differences in specific markers. Presence of stress responsive and pro-senescence marker p38 mitogen activated protein kinase (MAPK) and one of the DAMP) markers, HSP70, in exosomes from both control and CSE treated AECs. Expression of P-p38MAPK was higher in exosomes from AECs treated with CSE compared to control. AEC-amnion epithelial cell, CSE-cigarette smoke extract, DAMP-damage associated molecular pattern.

doi:10.1371/journal.pone.0157614.g002

treatment. We used two embryonic and amnion stem cell specific markers, Nanog (a transcription factor) and octamer-binding transcription factor 4 (Oct-4), to confirm origin of exosomes [49–54]. Although these two proteins are not exclusive to AECs, they are well documented in both amniotic epithelial and mesenchymal cells and are well reported to characterize AECs. AECs from both untreated and treated AECs demonstrated Nanog but Oct-4 was not localized in any of our exosome preparations.

We also used western blot analysis to detect the expression of Alix in AEC derived exosomes. As shown in Fig 2D, western blot analysis did not demonstrate the presence of Alix in either untreated or CSE treated AEC exosomes.

Flow cytometry was performed to further characterize the exosomes using tetraspanin markers CD9 and CD63 (Fig 2E), common markers used for exosome identification [55]. The shift in FITC intensity on the representative histograms in Fig 2E indicates beads positive for either CD9 or CD63 exosomes (pink peaks) relative to the negative control (no exosomes) (green peaks). By graphing forward scatter versus FITC intensity, we calculated the percentage of beads positive for exosome markers. After subtracting the negative control to account for background, results are expressed as percentage of beads positive for CD9 or CD63 expressing exosomes. Exosomes from control AECs showed an average of 70% for CD9 compared to 38% in CSE treated AEC exosomes. Similar decrease was also seen for CD63 (64% and 19% in controls vs CSE respectively). Difference in exosome marker expression was found to be statistically significant ($p < 0.05$).

Characterization of exosomal cargo from Control and CSE treated AECs

Western blot analysis showed the presence of active forms of pro-senescence and parturition associated marker p38 MAPK (P-p38 MAPK) and one of the damage associated molecular pattern (DAMP) molecule HSP70 in exosomes from both control and CSE treated AECs. As shown in Fig 1F HSP70, P-p38 MAPK and total p38 MAPK were seen in both untreated and treated exosomes. However, the intensity of bands for P-p38 MAPK was higher in exosomes from AECs treated with CSE.

Cell free fetal DNA are associated with human parturition through inflammatory activation [56]. Telomere fragments from fetal cells can also cause sterile inflammation in fetal tissues associated with parturition [13]. Exosomes are known to carry double and single stranded DNA fragments and cause immune activation in recipient cells [57]. Therefore, we examined untreated and CSE treated AEC derived exosomes for DNA fragments. Flow cytometry analysis for DNA content of exosomes from control and CSE treated cells (Fig 3) showed DNA within exosome preparations. There was no significant difference in DNA content between DNase treated and untreated nor between control and CSE treated AEC exosomes suggesting that external contaminant DNA are unlikely in our preparations and DNA fragmentation expected after CSE treatment did not result in increased exosomal content. We further confirmed the presence of DNA in both control and CSE exosomes by quantifying the amount of DNA using A260/280 and confirmed data obtained from flow cytometric analysis. Average DNA concentration from control exosomes was 4.7 ng/μL ± 0.794 while CSE exosomes averaged 5.1 ng/μL ± 1.86.

Immunofluorescence staining was used to colocalize markers within exosomes. As shown in Fig 4, HSC70 was colocalized with CD9 markers (Fig 4). The colocalizations were similar in both control and CSE treated AEC exosomes. This is also represented in the line graph of signal intensity over distance and bar graph representing mean Pearson's coefficient of colocalized volume from both control and CSE AEC exosomes. These findings suggest that HSC70 is a marker of AEC derived exosomes, confirming the western blot data.

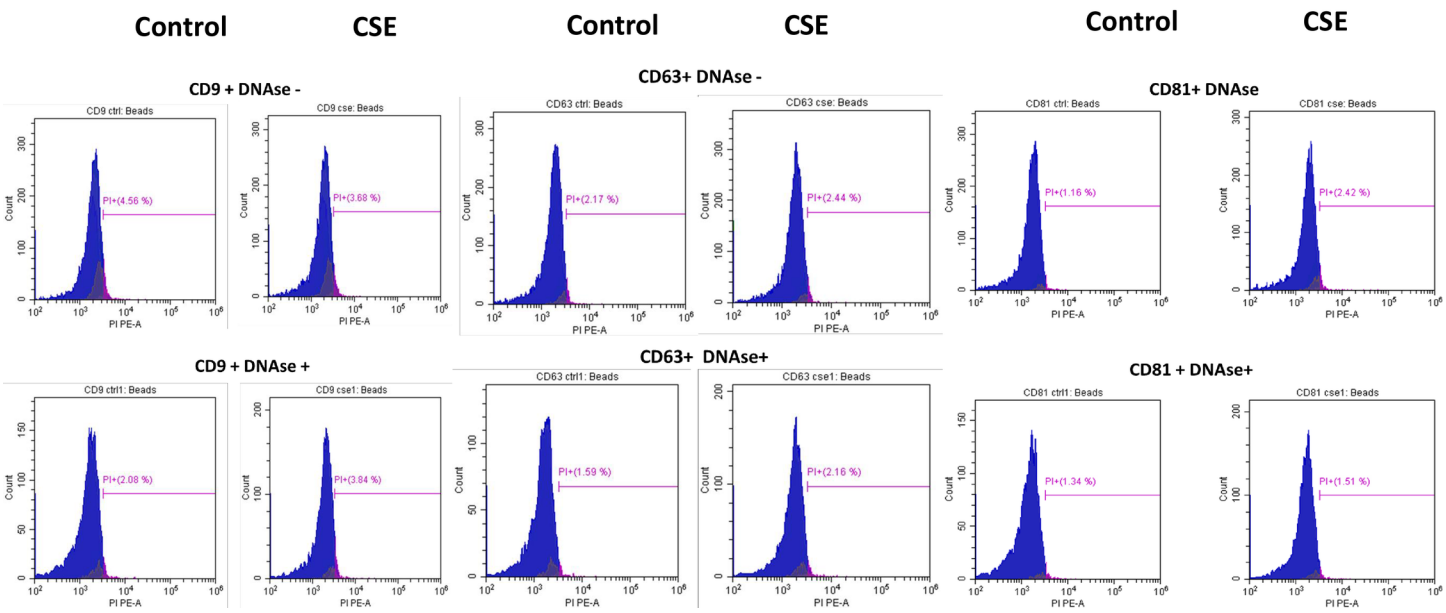

Fig 3. Documentation of DNA by flow cytometry in exosomes using propidium iodide (PI). There was no significant difference in DNA content in exosomes untreated with DNase (top) and those pretreated with DNase (bottom). There was also no significant difference in DNA content between CD9, CD63 and CD81 positive exosomes. The average DNA content was similar for both control (4.7 ng/μL) and CSE (5.1 ng/μL) derived exosomes. AEC-amnion epithelial cell, CSE-cigarette smoke extract.

doi:10.1371/journal.pone.0157614.g003

P-p38 MAPK (Fig 5), Histone 3 (H3, Fig 6), and HSP70 (Fig 7) were colocalized with exosome marker CD9 using immunofluorescent microscopy to determine whether exosomes reflect the physiologic state of AECs. All studied markers are associated with oxidative stress

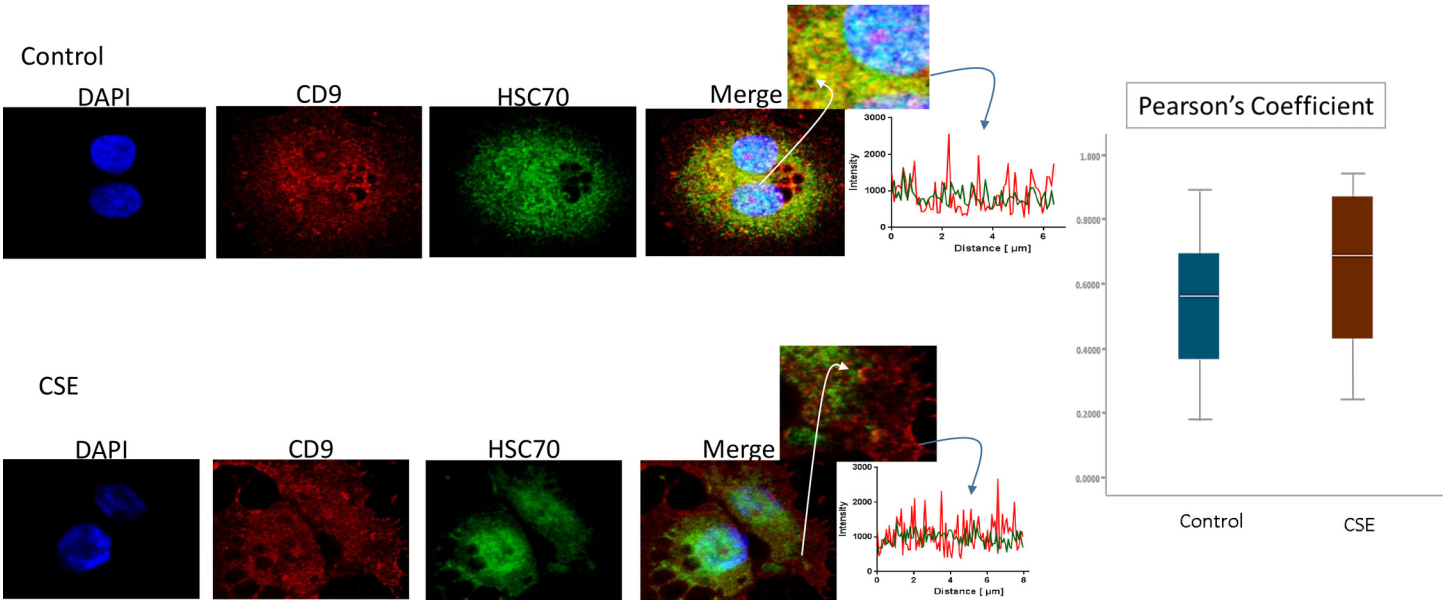

Fig 4. Colocalization of exosome marker HSC70 and CD9 in AECs. Control (untreated AECs) (top panel) have a similar amount of HSC70 (green) colocalization with CD9 exosome marker (red) compared to AECs exposed to CSE (bottom panel). The line graphs represent overlap between CD9 and HSC70 signal at the region of interest. The bar graph represents no significant differences between the two groups (Pearson's Coefficient p = ns). AEC-amnion epithelial cell, CSE-cigarette smoke extract.

doi:10.1371/journal.pone.0157614.g004

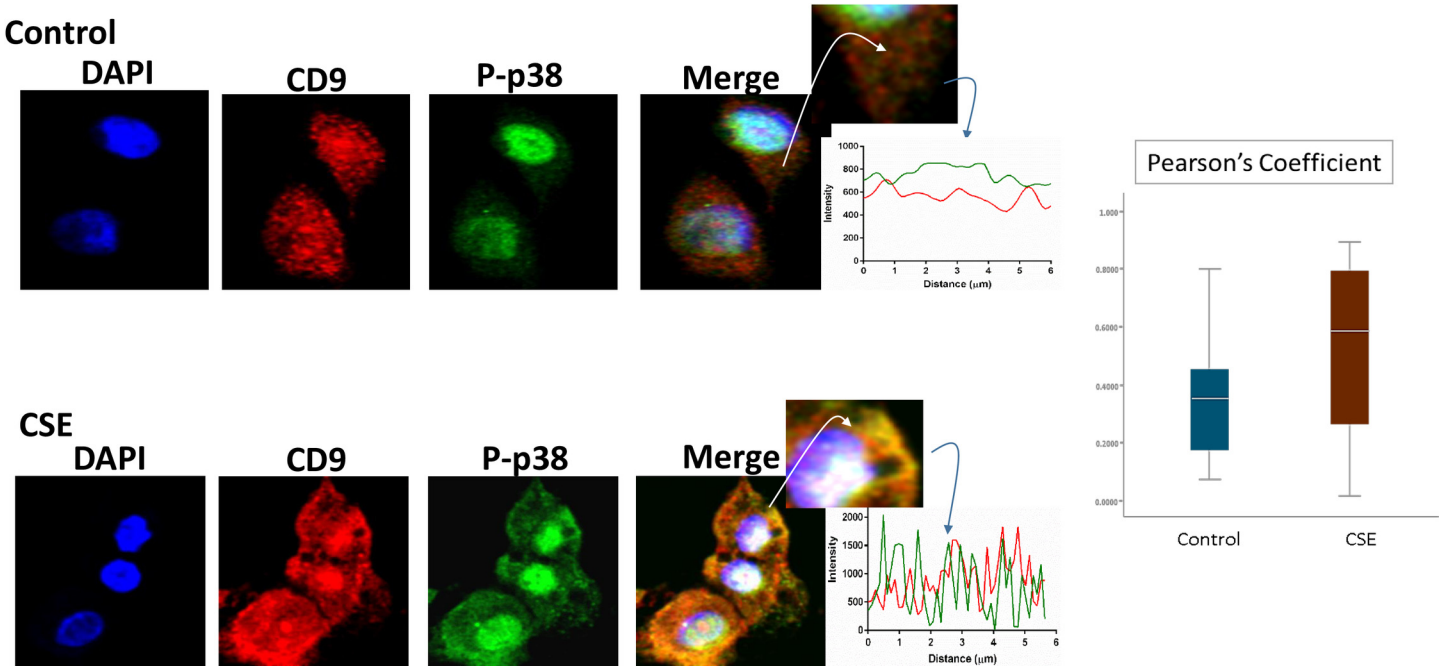

Fig 5. Colocalization of exosome marker H3 and CD9 in AECs. Immunofluorescence imaging of control (top panel) and CSE treated amnion cells (bottom panel) show colocalization differences of H3 (green) and CD9 (red). Significantly higher colocalization (line graph and bar graph) of H3 was seen after CSE treatment compared to control (Pearson's Coefficient P<0.0001) AEC-amnion epithelial cell, CSE-cigarette smoke extract.

doi:10.1371/journal.pone.0157614.g005

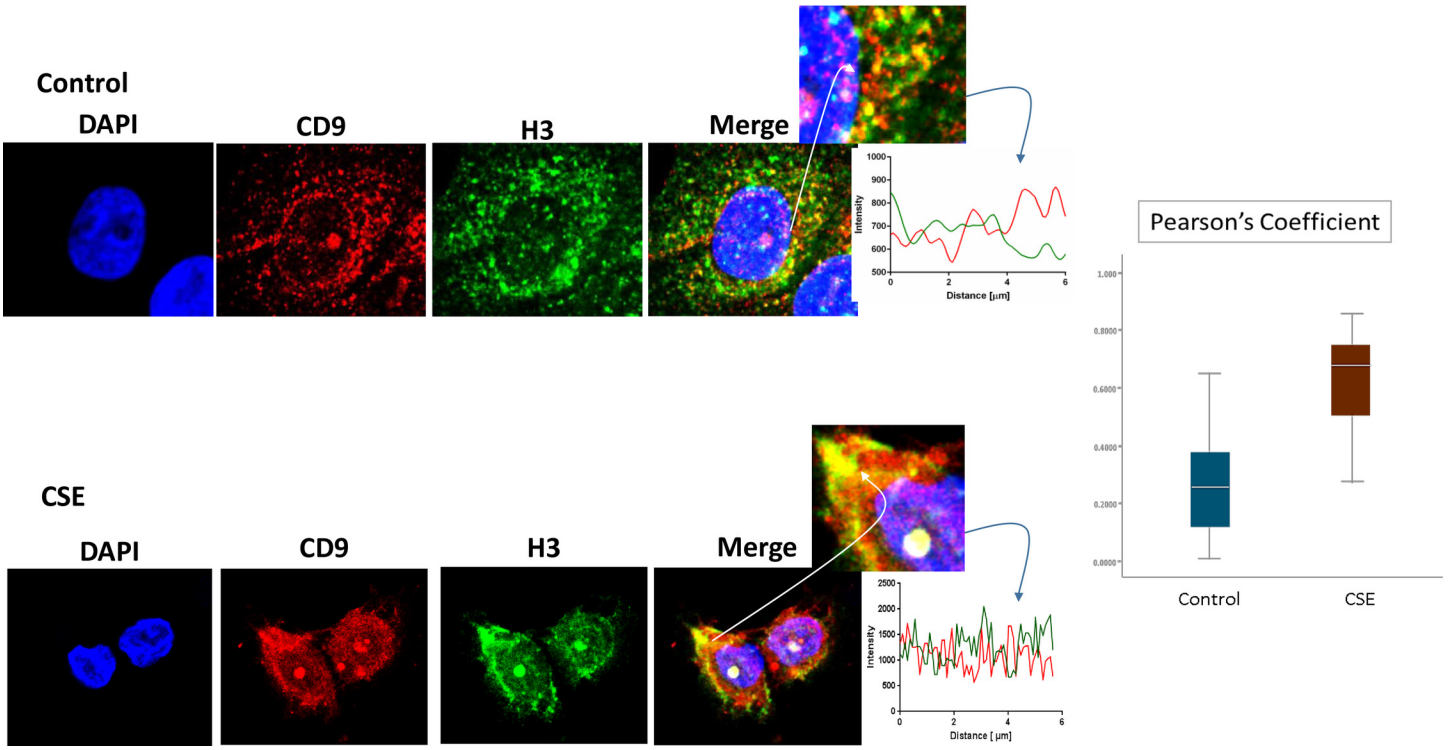

Fig 6. Colocalization of exosome marker HSP70 and CD9 in AECs. Colocalization of DAMP, HSP70, and CD9: Immunofluorescence imaging of control (top panel) and CSE treated amnion cells (bottom panel) show colocalization differences of HSP70 (green) and CD9 (red). Significantly higher colocalization (line graph and bar graph) of H3 was seen after CSE treatment compared to control (Pearson's Coefficient P<0.001) AEC-amnion epithelial cell, CSE-cigarette smoke extract; DAMP–Damage associated molecular pattern.

doi:10.1371/journal.pone.0157614.g006

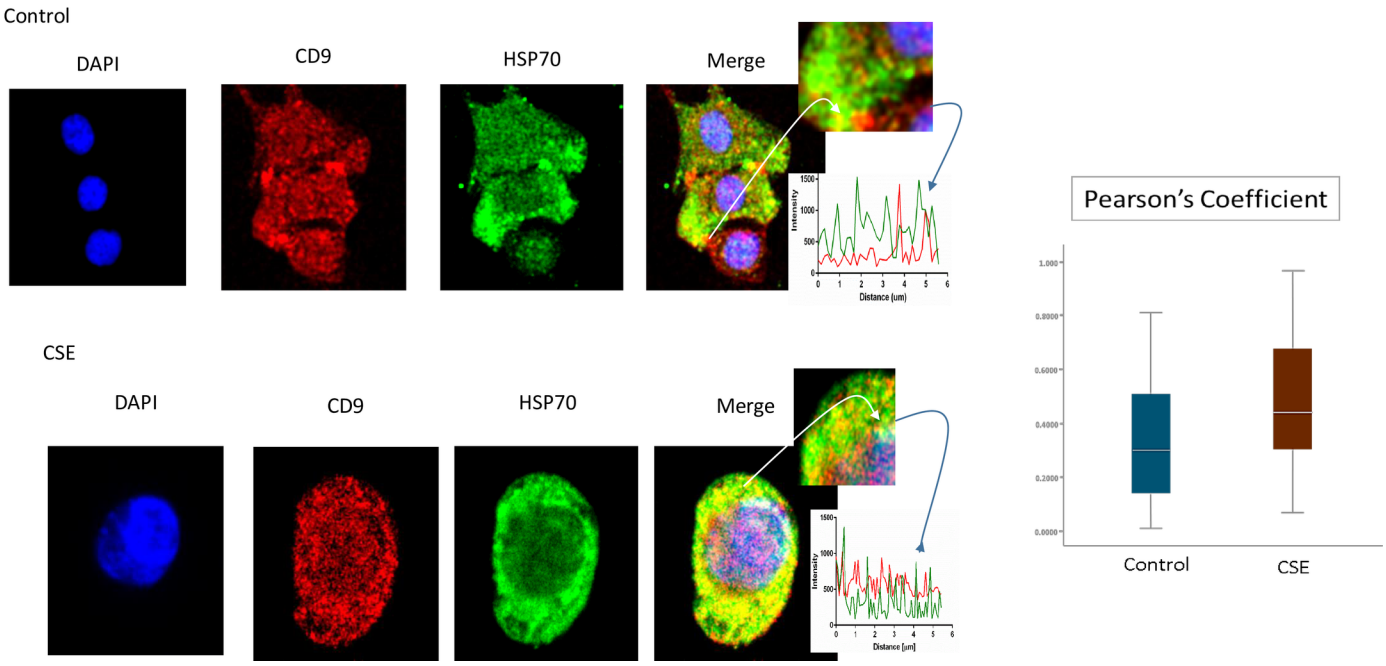

Fig 7. Colocalization of exosome marker P-p38MAPK and CD9 in AECs. Colocalization of pro-senescence marker P-p38MAPK and CD9: Immunofluorescence imaging of control (top panel) and CSE treated amnion cells (bottom panel) show colocalization differences of HSP70 (green) and CD9 (red). Significantly higher colocalization (line graph and bar graph) of H3 was seen after CSE treatment compared to control (Pearson's Coefficient P<0.0001) AEC-amnion epithelial cell, CSE-cigarette smoke extract.

doi:10.1371/journal.pone.0157614.g007

response and activation of p38 MAPK in amnion cells, which is the signaler in senescence response to CSE. H3 and HSP70 are p38 MAPK responder genes in stress associated cellular signaling [58,59]. Colocalization was quantified using Pearson's correlation coefficient and graphed comparing control and CSE mean values. Colocalization of all three markers were significantly higher in CSE treated AEC exosomes compared to control AEC exosomes (mean Pearson's correlation coefficients for each were statistically significant ($p<0.05$)) confirming CSE causes increased cargo of these markers by exosomes. CSE induced oxidative stress damage leads to senescence of AEC through p38 MAPK signaling (12] and current data confirm that P-p38 MAPK and its responder proteins H3 and HSP70 can also get packaged inside exosomes at a higher level reflecting the physiologic state of AECs.

Proteomic analysis of CTs-derived exosomes

Mass spectrometry analysis identified over 200 exosomal proteins (S1 Table). We also identified unique proteins for each condition (Fig 8A; Tables 2 and 3). The number of proteins identified in exosomes isolated from AEC exposed to CSE was higher (193) compared to control (173). We investigated the molecular network that can be activated by the proteins identified in exosomes isolated from AEC cultured under normal (8B) and oxidative stress conditions (8C). Interestingly, NF-κβ complex seems to be a central regulator in the molecular network that can be activated by exosomes from AEC cultured under normal conditions, where TGF-β might regulate the molecular network from exosomes from AEC treated with CSE. We have already reported that CSE treatment produce minimal activation of NF-κB compared to control and the exosomal proteomic analysis further supports our earlier findings [60]. We have also seen evidence of epithelial-mesenchymal transition (EMT) of amnion epithelial cells under oxidative stress conditions. TGF-β is a major mediator of EMT [61–65]. Molecular

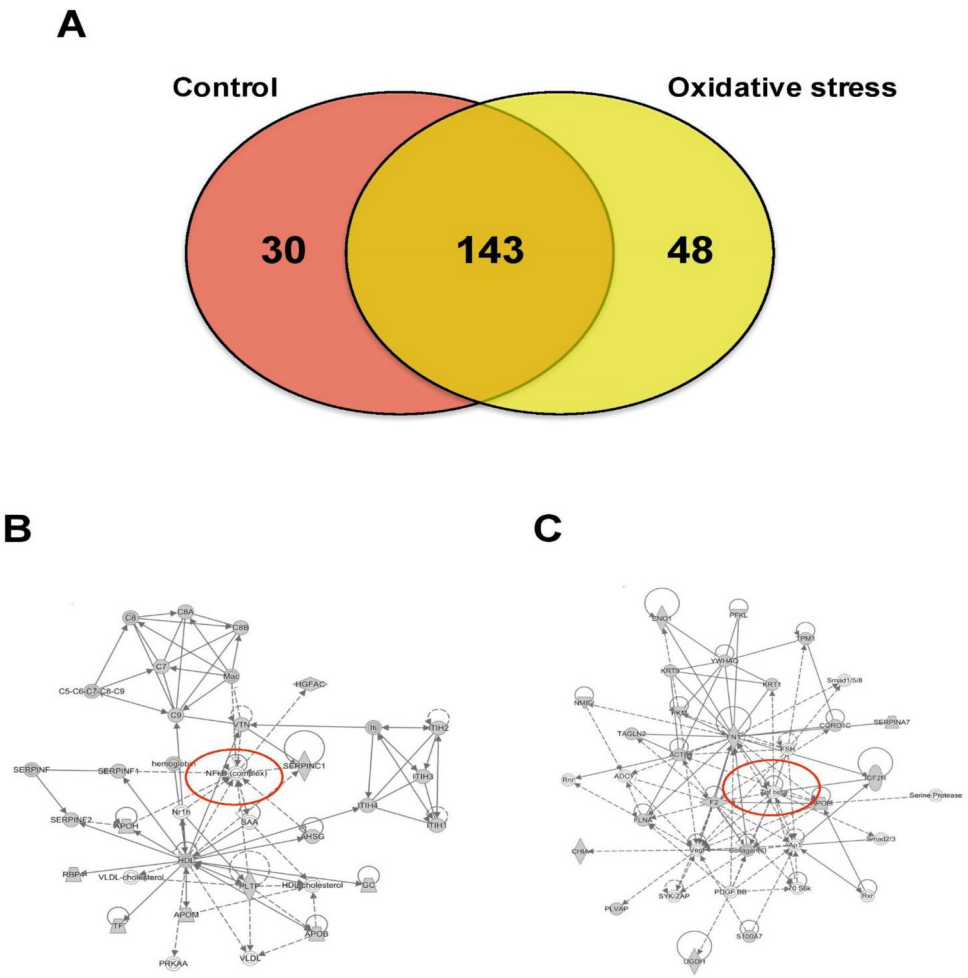

Fig 8. Proteomic analysis of AEC-derived exosome proteins. (A) The Venn diagram represents the distribution of common and unique proteins identified by nanospray LC-MS/MS in exosomes released from AEC cultured under normal or stress conditions. List contain 221 unique proteins. (B and C) Proteins identified in exosomes isolated from AEC under normal (B) or oxidative stress (C) conditions were submitted to IPA network analysis. Red circle: central molecules involved in the signaling pathways.

doi:10.1371/journal.pone.0157614.g008

networks in CSE treated exosomes confirms that TGF-β mediated EMT may be functional in AECs under oxidative stress. Using Ingenuity Pathway Analysis (IPA), a bioinformatics approach, we examined the biological pathways represented by differentially expressed proteins from our proteomic analysis. The canonical pathways determined by exosomal cargo contents showed ERK/MAPK (Fig 9A), PI3K/AKT (Fig 9B) and epithelial adherent junctions (Fig 9C) was significantly higher in exosomes from AEC under oxidative stress conditions compared to the control. On the other hand, canonical pathways as LPS/IL-1 mediated inhibition of the nuclear receptor retinoid X receptor (RXR) function and IL-6 signaling were significantly lower and unchanged in exosomes from AEC cultured under oxidative stress conditions compared to control, respectively. Finally, analysis of diseases and functions showed that exosomes isolated from AEC under oxidative stress conditions might significantly increase the eosinophilic inflammation compared to control. Interestingly, higher amount of eosinophil cells in the amniotic fluids has been associated with preterm labor [66].

Discussion

Ongoing studies suggest the development of fetal membrane senescence as a mechanism associated with term parturition [9,12,14]. Oxidative stress, antioxidant depletion, oxidative stress

Table 2. Proteomics analysis of exosomal cargo identified 30 unique markers in exosomes derived from amnion epithelial cells grown in normal culture conditions.

ID	Symbol	Entrez Gene Name	Function	Location
ADK_HUMAN	ADK	adenosine kinase	metabolism	Nucleus
AK1A1_HUMAN	AKR1A1	aldo-keto reductase family 1, member A1 (aldehyde reductase)	metabolism	Cytoplasm
ASSY_HUMAN	ASS1	argininosuccinate synthase 1	metabolism	Cytoplasm
CADH5_HUMAN	CDH5	cadherin 5	cell adhesion	Plasma Membrane
COBA1_HUMAN	COL11A1	collagen, type XI, alpha 1	cell adhesion	Extracellular Space
COR1A_HUMAN	CORO1A	coronin 1A	structural	Cytoplasm
DYH8_HUMAN	DNAH8	dynein, axonemal, heavy chain 8	structural	Cytoplasm
DESP_HUMAN	DSP	desmoplakin	cell adhesion	Plasma Membrane
URP2_HUMAN	FERMT3	fermitin family member 3	cell adhesion	Cytoplasm
FMOD_HUMAN	FMOD	fibromodulin	structural	Extracellular Space
GSTA2_HUMAN	GSTA2	glutathione S-transferase alpha 2	metabolism	Cytoplasm
HGD_HUMAN	HGD	homogentisate 1,2-dioxygenase	metabolism	Cytoplasm
HORN_HUMAN	HRNR	hornerin	structural	Cytoplasm
IBP7_HUMAN	IGFBP7	insulin like growth factor binding protein 7	cell adhesion	Extracellular Space
KPRP_HUMAN	KPRP	keratinocyte proline-rich protein	other	Cytoplasm
LYSC_HUMAN	LYZ	lysozyme	immune response	Extracellular Space
MAOX_HUMAN	ME1	malic enzyme 1, NADP (+)-dependent, cytosolic	metabolism	Cytoplasm
NCAM1_HUMAN	NCAM1	neural cell adhesion molecule 1	cell adhesion	Plasma Membrane
NELL2_HUMAN	NELL2	neural EGFL like 2	cell adhesion	Extracellular Space
PARVA_HUMAN	PARVA	parvin alpha	cell adhesion	Cytoplasm
PROF1_HUMAN	PFN1	profilin 1	cell adhesion	Cytoplasm
PROS_HUMAN	PROS1	protein S (alpha)	cell migration	Extracellular Space
PYGB_HUMAN	PYGB	phosphorylase, glycogen; brain	metabolism	Cytoplasm
S10A8_HUMAN	S100A8	S100 calcium binding protein A8	inflammation	Cytoplasm
HEP2_HUMAN	SERPIND1	serpin peptidase inhibitor, clade D (heparin cofactor), member 1	cell migration	Extracellular Space
SHBG_HUMAN	SHBG	sex hormone-binding globulin	transport	Extracellular Space
SPRR3_HUMAN	SPRR3	small proline-rich protein 3	structural	Cytoplasm
ST1E1_HUMAN	SULT1E1	sulfotransferase family 1E member 1	metabolism	Cytoplasm
VCAM1_HUMAN	VCAM1	vascular cell adhesion molecule 1	cell adhesion	Plasma Membrane
VNN1_HUMAN	VNN1	vanin 1	cell adhesion	Plasma Membrane

doi:10.1371/journal.pone.0157614.t002

Table 3. Proteomics analysis of exosomal cargo identified 48 unique markers in exosomes derived from amnion epithelial cells grown under oxidative stress conditions.

ID	Symbol	Entrez Gene Name	Function (UniProt)	Location
ACES_HUMAN	ACHE	acetylcholinesterase (Yt blood group)	signaling	Plasma Membrane
ACTN1_HUMAN	ACTN1	actinin, alpha 1	structural	Cytoplasm
AOC3_HUMAN	AOC3	amine oxidase, copper containing 3	cell adhesion	Plasma Membrane
APOA4_HUMAN	APOA4	apolipoprotein A-IV	binding protein	Extracellular Space
RIMB1_HUMAN	BZRAP1	benzodiazepine receptor (peripheral) associated protein 1	binding protein	Cytoplasm
CR063_HUMAN	C18orf63	chromosome 18 open reading frame 63	Other	Other
CO2_HUMAN	C2	complement component 2	immune response	Extracellular Space
CAB39_HUMAN	CAB39	calcium binding protein 39	cell cycle	Cytoplasm
CADH6_HUMAN	CDH6	cadherin 6	cell adhesion	Plasma Membrane
CFAB_HUMAN	CFB	complement factor B	immune response	Extracellular Space
CNDP2_HUMAN	CNDP2	CNDP dipeptidase 2 (metallopeptidase M20 family)	cell cycle	Cytoplasm
COR1C_HUMAN	CORO1C	coronin 1C	signaling	Cytoplasm
DPYS_HUMAN	DPYS	dihydropyrimidinase	metabolism	Cytoplasm
FILA_HUMAN	FLG	filaggrin	structural	Cytoplasm
FILA2_HUMAN	FLG2	filaggrin family member 2	structural	Cytoplasm
GDIB_HUMAN	GDI2	GDP dissociation inhibitor 2	signaling	Cytoplasm
GSTM5_HUMAN	GSTM5	glutathione S-transferase mu 5	metabolism	Cytoplasm
HS90B_HUMAN	HSP90AB1	heat shock protein 90kDa alpha family class B member 1	inflammation	Cytoplasm
IGF2_HUMAN	IGF2	insulin like growth factor 2	signaling	Extracellular Space
ITA2_HUMAN	ITGA2	integrin subunit alpha 2	cell adhesion	Plasma Membrane
LAMC1_HUMAN	LAMC1	laminin subunit gamma 1	cell adhesion	Extracellular Space
MYH2_HUMAN	MYH2	myosin, heavy chain 2, skeletal muscle, adult	structural	Cytoplasm
NDKB_HUMAN	NME2	NME/NM23 nucleoside diphosphate kinase 2	metabolism	Nucleus
PCLO_HUMAN	PCLO	piccolo presynaptic cytomatrix protein	signaling	Cytoplasm
PFKAL_HUMAN	PFKL	phosphofructokinase, liver	metabolism	Cytoplasm
PAFA_HUMAN	PLA2G7	phospholipase A2 group VII	inflammation	Extracellular Space
PLVAP_HUMAN	PLVAP	plasmalemma vesicle associated protein	signaling	Plasma Membrane
PPIB_HUMAN	PPIB	peptidylprolyl isomerase B	structural	Cytoplasm
PRDX1_HUMAN	PRDX1	peroxiredoxin 1	inflammation	Cytoplasm
PRDX2_HUMAN	PRDX2	peroxiredoxin 2	inflammation	Cytoplasm
PSA1_HUMAN	PSMA1	proteasome subunit alpha 1	cell cycle	Cytoplasm
PSA4_HUMAN	PSMA4	proteasome subunit alpha 4	cell cycle	Cytoplasm

(*Continued*)

Table 3. (*Continued*)

ID	Symbol	Entrez Gene Name	Function (UniProt)	Location
PSA6_HUMAN	PSMA6	proteasome subunit alpha 6	cell cycle	Cytoplasm
PSA7_HUMAN	PSMA7	proteasome subunit alpha 7	cell cycle	Cytoplasm
PSMD5_HUMAN	PSMD5	proteasome 26S subunit, non-ATPase 5	cell cycle	Other
PYGL_HUMAN	PYGL	phosphorylase, glycogen, liver	metabolism	Cytoplasm
RAN_HUMAN	RAN	RAN, member RAS oncogene family	cell cycle	Nucleus
RAP1B_HUMAN	RAP1B	RAP1B, member of RAS oncogene family	transport	Cytoplasm
S10A7_HUMAN	S100A7	S100 calcium binding protein A7	inflammation	Cytoplasm
S10A9_HUMAN	S100A9	S100 calcium binding protein A9	inflammation	Cytoplasm
TAGL2_HUMAN	TAGLN2	transgelin 2	binding	Cytoplasm
TFR1_HUMAN	TFRC	transferrin receptor	transport	Plasma Membrane
TENX_HUMAN	TNXB	tenascin XB	cell adhesion	Extracellular Space
TPM1_HUMAN	TPM1	tropomyosin 1 (alpha)	structural	Cytoplasm
TBA4A_HUMAN	TUBA4A	tubulin alpha 4a	structural	Cytoplasm
RL40_HUMAN	UBA52	ubiquitin A-52 residue ribosomal protein fusion product 1	inflammation	Cytoplasm
WDR1_HUMAN	WDR1	WD repeat domain 1	transport	Extracellular Space
1433T_HUMAN	YWHAQ	tyrosine 3-monooxygenase/ tryptophan 5-monooxygenase activation protein, theta	signaling	Cytoplasm

doi:10.1371/journal.pone.0157614.t003

induced senescence, stress associated p38 MAPK activation, and sterile inflammation, are associated with normal term human parturition [9,12,67,68]. These findings in *in vivo* clinical samples were recapitulated in vitro using normal term not in labor fetal membrane explant cultures or AECs where oxidative stress induced transition of fetal membranes to a senescence phenotype mimicked term labor status [12–14]. This suggests that exogenous oxidative stress at term promotes senescence and senescent fetal membrane cells to signal parturition by enhancing the overall inflammatory load in the uterine cavity. In this study, we demonstrated that AEC-derived exosomes may serve as carriers of signals of communication between various tissue layers by senescent fetal cells. Exosomes, generated as a consequence of multivesicular endosome (MVE) fusion with the plasma membranes [69–71], and their contents (protein, DNA, and all forms of RNAs), represent the character and physiologic state of the cell of origin that makes them good vectors of paracrine signaling.

The primary aim of this study was to isolate, characterize and demonstrate that AEC derived exosomes reflect the physiological status of the cells of origin. Our key findings are as follows: 1) AEC derived exosomes demonstrated classic shape, size and markers (CD9, 63, 81, HSC 70) along with amnion cell-stem cell specific transcription factor Nanog, regardless of treatment. 2) AEC derived exosomes do not show the presence of ESCRT-associated protein Alix and amnion cell stem cell marker Oct-4 in their cargo. 3) CSE treatment caused increased

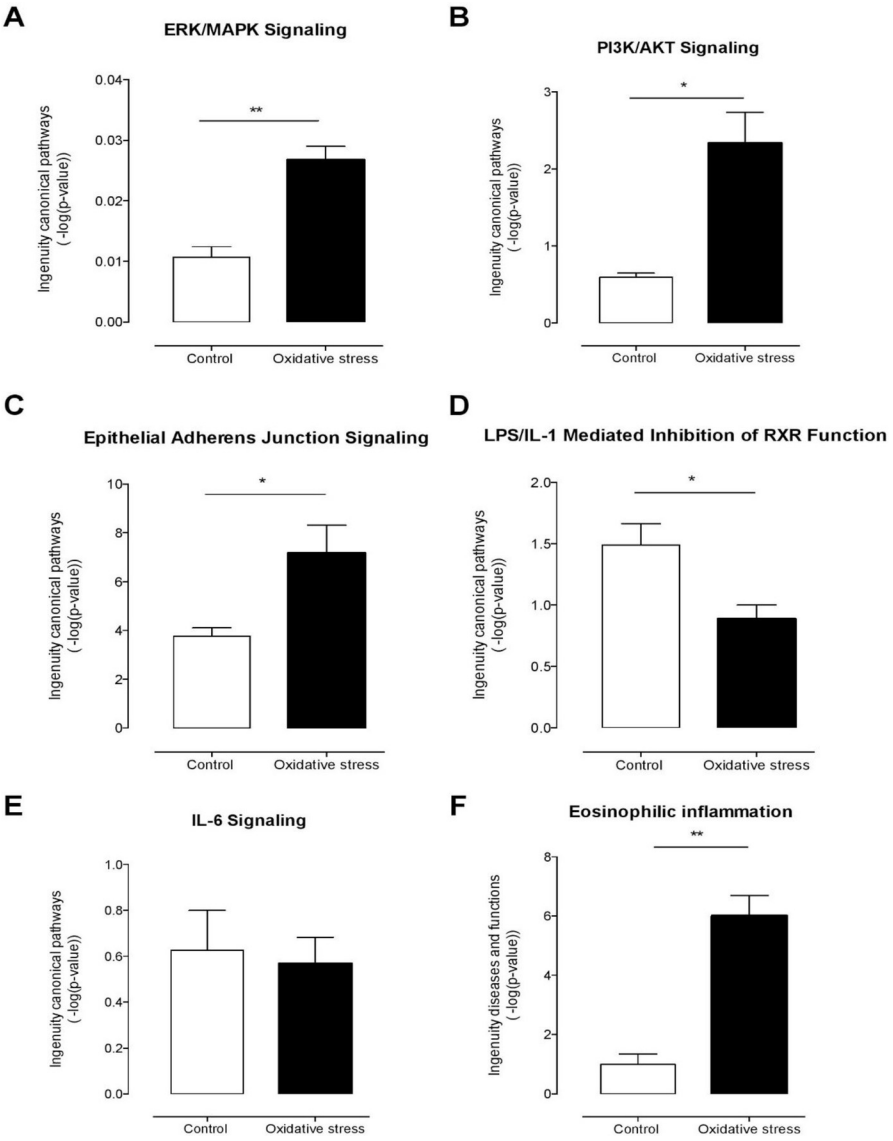

Fig 9. Ingenuity pathway analysis of AEC-derived-exosomes proteins. Exosomal protein identified under normal (control) or oxidative stress conditions were analyzed using the IPA software. Comparison of canonical pathways: (A) ERK/MAPK, (B) PI3K/AKT, (C) epithelial adherens junctions, (D) LPS/IL-1 mediated inhibition of RXR function and (E) IL-6 signaling. Diseases and functions analysis: (F) eosinophilic inflammation. Values are mean ± SD. In A and F, **p < 0.001. In B, C and D, *p < 0.005.

doi:10.1371/journal.pone.0157614.g009

colocalization of H3, HSP70 and active p38 (P-p38) MAPK in AEC exosomes. Increased localization of these proteins demonstrated a pathophysiological phenotype of AECs in response to CSE induced oxidative stress. Although the functional relevance is unclear, this is the first report to demonstrate P-p38 MAPK as an exosomal cargo. We propose that AEC-derived exosomes demonstrate the characteristics of a pathophysiological state of the cell of origin and that the presence of P-p38 MAPK, a marker of inflammation, is a key mediator of senescence induction and sterile inflammation. Our studies suggest the importance of AEC derived exosome cargo in causing potential functional changes in feto-maternal compartments. Although we do not report any functional role of AEC exosomes during pregnancy, ongoing research is focused on determining such a role.

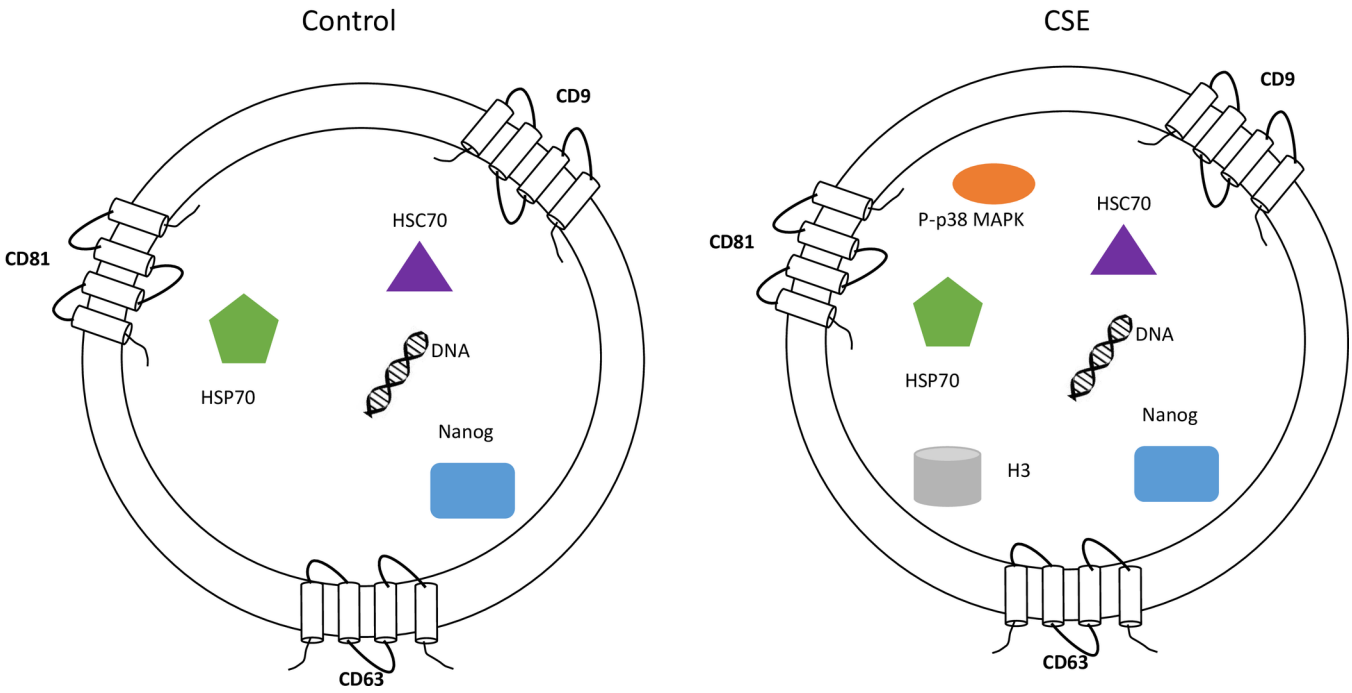

Fig 10. Characterization of AEC exosomes. The exosomes isolated from untreated (control) and CSE treated primary AEC carry cargo representative of the state of the origin cell. AEC exosomes contain tetraspnins (CD9, CD63 and CD81), Nanog, HSC70, HSP70 and DNA regardless of treatment, while CSE exosomes contain significantly increased amounts of P-p38MAPK and H3 compared with control exosomes.

doi:10.1371/journal.pone.0157614.g010

The impact of p38 MAPK activation is well documented in fetal tissues but no data exist on its functional contributions on myometrial side whose contractility determines pregnancy outcome. Functional progesterone withdrawal and subsequent myometrial activation (i.e. increased contractility and excitability) are key events in the initiation of labor [72–75]. Functional progesterone withdrawal, which is mediated, in part, by switching of the PR-A:PR-B ratio in myometrial cells from PR-B-dominance (mediates anti-inflammatory and relaxing actions of progesterone) to PR-A-dominance (inhibits the anti-inflammatory actions of progesterone and increase contractility) [72–75]. A key finding in breast cancer cell lines is that the PR-A: PR-B ratio is determined by the stability of the PR-A and PR-B proteins, which is caused by post-translational modifications, especially phosphorylation by MAPKs at specific serine residues in the N-terminal domain [76–79]. Khan et al found that PR-A stability is increased by MEKK1-induced p38 MAPK activation, which increased the PR-A: PR-B ratio; whereas PR-B stability was increased by activation of ERK1/2, leading to a decrease in the PR-A: PR-B ratio. Our unpublished data (performed in collaboration with Dr. Sam Mesiano) in myometrial cells demonstrate that CSE can cause functional progesterone withdrawal in myocytes through p38 MAPK mediated mechanism, a process reversed by p38 MAPK inhibitor SB203580. This determined the impact of p38 MAPK in human parturition. Therefore exosomal transport of fetal cell derived P-p38 MAPK to the maternal side may be influential in determining the status of pregnancy. This is also dependent on the number of exosomes and load of p38 MAPK that can reach the maternal side. Exosomes may carry other inflammatory molecules (SASP) from senescent fetal cells and they may also enhance the inflammatory load on the maternal side. We postulate that based on the physiologic state of cell, exosome cargo and signaling may determine the outcome of pregnancy. Placental derived exosomes have been well documented in maternal liquid biopsies and their changes (quantity and contents) have been implicated in various pregnancy associated pathologies [31–37,40,42,46–48,80–94].

Although AEC exosomes demonstrated the consistent presence of classical exosomal markers and the amnion stem cell marker Nanog, we did not show one of the ESCRT class of proteins, Alix. ESCRT complex dependent and independent mechanisms of exosomal assembly and secretion have been described as a tissue/cell specific physiological phenomenon [27]. Based on our experimental approaches, AEC exosomes are likely derived without the participation of the ESCRT protein; however, we do not rule out mediation by other classes of ESCRT proteins. We have documented three of the tetraspanin protein markers (CD9, CD63 and CD81) that can participate in exosomal assembly and release of cargo.

In summary, we have demonstrated AECs produce exosomes and that their cargo reflects the status of the cell (Fig 10). Furthermore, we identified active p38 MAPK as one of the cargo proteins in exosomes derived from oxidative stress-treated AECs. Our studies highlight the significance of AEC derived exosomes as donors of p38 MAPK which plays a major role in determining the fate of pregnancy. This study demonstrated a limited number of markers and further characterization of AEC exosome cargo using proteomic approaches are warranted to elucidate the functional role of exosomes in human parturition and feto-maternal communication.

Supporting Information

S1 Table. Proteomics analysis of exosomal cargo identified over 200 proteins in exosomes derived from amnion epithelial cells grown under control and oxidative stress conditions.
(DOCX)

Acknowledgments

Authors acknowledge support by all the staff from the Maternal-Fetal Medicine and Perinatal Research Laboratory, University of Texas Medical Branch at Galveston (UTMB), TX, USA. We specifically acknowledge the contributions of Talar Kechichian, MS, (laboratory manager) for her expertise in protein chemistry and western blot analysis of samples, Jayshil Trivedi, MS for providing cell and molecular biological expertise.

TEM was performed at the electron microscopy core laboratory at UTMB with support and guidance from Dr. Michael Woodson, PhD.

This study is supported by Innovative catalyst grant funding from March of Dimes Center of Ohio, Cincinnati, OH to R Menon and partially by R. Menon's Faculty development funds from University of Texas Medical Branch at Galveston, TX. Authors declare all the funding or sources of support received during this specific study. The funders had no role in study design, data collection and analysis, decision to publish, or preparation of the manuscript.

Author Contributions

Conceived and designed the experiments: RM. Performed the experiments: SS LR RU. Analyzed the data: RM SS CS. Contributed reagents/materials/analysis tools: RM JP CS GRS. Wrote the paper: RM SS JP CS.

References

1. Casey ML, Macdonald PC. The endocrinology of human parturition. Ann N Y Acad Sci. 1997; 828: 273–84. PMID: 9329848
2. Challis JRG, Bloomfield FH, Booking AD, Casciani V, Chisaka H, Connor K, et al. Fetal signals and parturition. J Obstet Gynaecol Res. 2005; 31: 492–9. PMID: 16343248
3. Romero R, Dey SK, Fisher SJ. Preterm Labor: One Syndrome, Many Causes. Science. 2014; 345: 760–5. doi: 10.1126/science.1251816 PMID: 25124429

4. Smith R, Mesiano S, McGrath S. Hormone trajectories leading to human birth. Regul Pept. 2002; 108: 159–64. PMID: 12220740
5. Phaneuf S. AGLBARJE-FG. Parturition: activation of stimulatory pathways or loss of uterine quiescence? Adv Exp Med Biol. 1995; 395: 435–51. PMID: 8713997
6. Blackburn S. Maternal, Fetal, & Neonatal Physiology. Elsevier Health Sciences; 2014. 768 p.
7. Shynlova O, Tsui P, Jaffer S, Lye SJ. Integration of endocrine and mechanical signals in the regulation of myometrial functions during pregnancy and labour. Eur J Obstet Gynecol Reprod Biol. 2009; 144: S2–10. doi: 10.1016/j.ejogrb.2009.02.044 PMID: 19299064
8. Shynlova O, Lee Y-H, Srikhajon K, Lye SJ. Physiologic uterine inflammation and labor onset: integration of endocrine and mechanical signals. Reprod Sci. 2013; 20: 154–67. doi: 10.1177/1933719112446084 PMID: 22614625
9. Behnia F, Taylor BD, Woodson M, Kacerovský M, Hawkins H, Fortunato SJ, et al. Chorioamniotic membrane senescence: a signal for parturition? Am J Obstet Gynecol. 2015; 213: 1–16.
10. Fox H, Faulk WP. The placenta as an experimental model. Clin Endocrinol Metab. 1981; 10: 57–72. PMID: 6261997
11. Menon R, Yu J, Basanta-Henry P, Brou L, Berga SL, Fortunato SJ, et al. Short fetal leukocyte telomere length and preterm prelabor rupture of the membranes. PLoS One. 2012; 7: 1–6.
12. Menon R, Boldogh I, Urrabaz-Garza R, Polettini J, Syed TA, Saade GR, et al. Senescence of primary amniotic cells via oxidative DNA damage. PLoS One. 2013; 8: e83416. doi: 10.1371/journal.pone.0083416 PMID: 24386195
13. Polettini J, Behnia F, Taylor BD, Saade GR, Taylor RN, Menon R. Telomere Fragment Induced Amnion Cell Senescence: A Contributor to Parturition? Sun K, editor. PLoS One. 2015; 10: e0137188. doi: 10.1371/journal.pone.0137188 PMID: 26397719
14. Menon R, Boldogh I, Hawkins HK, Woodson M, Polettini J, Syed TA, et al. Histological Evidence of Oxidative Stress and Premature Senescence in Preterm Premature Rupture of the Human Fetal Membranes Recapitulated in Vitro. Am J Pathol. 2014; 184: 1740–51. doi: 10.1016/j.ajpath.2014.02.011 PMID: 24832021
15. Coppé J-P, Desprez P-Y, Krtolica A, Campisi J. The Senescence-Associated Secretory Phenotype: The Dark Side of Tumor Suppression. Annu Rev Pathol Mech Dis. 2010; 5: 99–118.
16. Bredeson S, Papaconstantinou J, Deford JH, Kechichian T, Syed TA, Saade GR, et al. HMGB1 promotes a p38MAPK associated non-infectious inflammatory response pathway in human fetal membranes. PLoS One. 2014; 9: e113799. doi: 10.1371/journal.pone.0113799 PMID: 25469638
17. De Toro J, Herschlik L, Waldner C, Mongini C. Emerging Roles of Exosomes in Normal and Pathological Conditions: New Insights for Diagnosis and Therapeutic Applications. Front Immunol. 2015; 6: 1–12.
18. Luo S-S, Ishibashi O, Ishikawa G, Ishikawa T, Katayama A, Mishima T, et al. Human Villous Trophoblasts Express and Secrete Placenta-Specific MicroRNAs into Maternal Circulation via Exosomes. Biol Reprod. 2009; 81: 717–29. doi: 10.1095/biolreprod.108.075481 PMID: 19494253
19. Zhang B, Yin Y, Lai RC, Lim SK. Immunotherapeutic Potential of Extracellular Vesicles. Front Immunol. 2014; 5: 1–11.
20. Buzas EI, György B, Nagy G, Falus A, Gay S. Emerging role of extracellular vesicles in inflammatory diseases. Nat Rev Rheumatol. 2014; 10: 356–64. doi: 10.1038/nrrheum.2014.19 PMID: 24535546
21. Liga A, Vliegenthart ADB, Oosthuyzen W, Dear JW, Kersaudy-Kerhoas M. Exosome isolation: a microfluidic road-map. Lab Chip. 2015; 15: 2388–94. doi: 10.1039/c5lc00240k PMID: 25940789
22. Lin J, Li J, Huang B, Liu J, Chen X, Chen X-M, et al. Exosomes: novel biomarkers for clinical diagnosis. ScientificWorldJournal. 2015; 2015: 657086. doi: 10.1155/2015/657086 PMID: 25695100
23. Frydrychowicz M, Kolecka-Bednarczyk a, Madejczyk M, Yasar S, Dworacki G. Exosomes—Structure, Biogenesis and Biological Role in Non-Small-Cell Lung Cancer. Scand J Immunol. 2015; 81: 2–10. doi: 10.1111/sji.12247 PMID: 25359529
24. Cai X, Janku F, Zhan Q, Fan J-B. Accessing Genetic Information with Liquid Biopsies. Trends Genet. 2015; 31: 564–75. doi: 10.1016/j.tig.2015.06.001 PMID: 26450339
25. Rana S, Zöller M. Exosome target cell selection and the importance of exosomal tetraspanins: a hypothesis. Biochem Soc Trans. 2011; 39: 559–62. doi: 10.1042/BST0390559 PMID: 21428939
26. Raposo G, Stoorvogel W. Extracellular vesicles: Exosomes, microvesicles, and friends. J Cell Biol. 2013; 200: 373–83. doi: 10.1083/jcb.201211138 PMID: 23420871
27. Stoorvogel W, Kleijmeer MJ, Geuze HJ, Raposo G. The biogenesis and functions of exosomes. Traffic. 2002; 3: 321–30. PMID: 11967126

28. Urbanelli L, Magini A, Buratta S, Brozzi A, Sagini K, Polchi A, et al. Signaling pathways in exosomes biogenesis, secretion and fate. Genes. 2013; 4: 152–70. doi: 10.3390/genes4020152 PMID: 24705158

29. Corrado C, Raimondo S, Chiesi A, Ciccia F, De Leo G, Alessandro R. Exosomes as intercellular signaling organelles involved in health and disease: Basic science and clinical applications. Int J Mol Sci. 2013; 14: 5338–66. doi: 10.3390/ijms14035338 PMID: 23466882

30. Bobrie A, Colombo M, Raposo G, Théry C. Exosome Secretion: Molecular Mechanisms and Roles in Immune Responses. Traffic. 2011; 12: 1659–68. doi: 10.1111/j.1600-0854.2011.01225.x PMID: 21645191

31. Mitchell MD, Peiris HN, Kobayashi M, Koh YQ, Duncombe G, Illanes SE, et al. Placental exosomes in normal and complicated pregnancy. Am J Obstet Gynecol. 2015; 213: S173–81. doi: 10.1016/j.ajog.2015.07.001 PMID: 26428497

32. Sabapatha A, Gercel-taylor C, Taylor DD. Specific isolation of placenta-derived exosomes from the circulation of pregnant women and their immunoregulatory consequences. Am J Reprod Immunol. 2006; 56: 345–55. PMID: 17076679

33. Salomon C, Torres MJ, Kobayashi M, Scholz-Romero K, Sobrevia L, Dobierzewska A, et al. A gestational profile of placental exosomes in maternal plasma and their effects on endothelial cell migration. PLoS One. 2014; 9: e98667. doi: 10.1371/journal.pone.0098667 PMID: 24905832

34. Salomon C, Yee S, Scholz-Romero K, Kobayashi M, Vaswani K, Kvaskoff D, et al. Extravillous trophoblast cells-derived exosomes promote vascular smooth muscle cell migration. Front Pharmacol. 2014; 5: 175. doi: 10.3389/fphar.2014.00175 PMID: 25157233

35. Sarker S, Scholz-Romero K, Perez A, Illanes SE, Mitchell MD, Rice GE, et al. Placenta-derived exosomes continuously increase in maternal circulation over the first trimester of pregnancy. J Transl Med. 2014; 12: 204. doi: 10.1186/1479-5876-12-204 PMID: 25104112

36. Ouyang Y, Mouillet JF, Coyne CB, Sadovsky Y. Review: Placenta-specific microRNAs in exosomes—Good things come in nano-packages. Placenta. 2014; 35: S69–73. doi: 10.1016/j.placenta.2013.11.002 PMID: 24280233

37. Donker RB, Mouillet JF, Chu T, Hubel CA, Stolz DB, Morelli AE, et al. The expression profile of C19MC microRNAs in primary human trophoblast cells and exosomes. Mol Hum Reprod. 2012; 18;: 417–24. doi: 10.1093/molehr/gas013 PMID: 22383544

38. Sadovsky Y, Mouillet J, Ouyang Y, Bayer A. The Function of TrophomiRs and Other MicroRNAs in the Human Placenta. Cold Spring Harb Perspect Med. 2015; 5: a023036. doi: 10.1101/cshperspect.a023036 PMID: 25877393

39. Salomon C, Scholz-Romero K, Sarker S, Sweeney E, Kobayashi M, Correa P, et al. Gestational Diabetes Mellitus Is Associated With Changes in the Concentration and Bioactivity of Placenta-Derived Exosomes in Maternal Circulation Across Gestation. Diabetes. 2016; 65: 598–609. doi: 10.2337/db15-0966 PMID: 26718504

40. Rice GE, Scholz-Romero K, Sweeney E, Peiris H, Kobayashi M, Duncombe G, et al. The Effect of Glucose on the Release and Bioactivity of Exosomes From First Trimester Trophoblast Cells. J Clin Endocrinol Metab. 2015; 100: E1280–8. doi: 10.1210/jc.2015-2270 PMID: 26241326

41. Salomon C, Kobayashi M, Ashman K, Sobrevia L, Mitchell MD, Rice GE. Hypoxia-induced changes in the bioactivity of cytotrophoblast-derived exosomes. PLoS One. 2013; 8: e79636. doi: 10.1371/journal.pone.0079636 PMID: 24244532

42. Salomon C, Ryan J, Sobrevia L, Kobayashi M, Ashman K, Mitchell M, et al. Exosomal Signaling during Hypoxia Mediates Microvascular Endothelial Cell Migration and Vasculogenesis. PLoS One. 2013; 8: 1–24.

43. Polettini J, Silva MG, Kacerovsky M, Syed TA, Saade G, Menon R. Expression profiles of fetal membrane nicotinamide adenine dinucleotide phosphate oxidases (NOX) 2 and 3 differentiates spontaneous preterm birth and pPROM pathophysiologies. Placenta. 2014; 35: 188–94. doi: 10.1016/j.placenta.2013.12.012 PMID: 24439294

44. Polettini J, Silva M, Syed T, Saade G, Menon R. 828: Screening of lysyl oxidase (LOX) and lysyl oxidase-like (LOXL) enzyme expression and activity in human fetal membranes. Am J Obstet Gynecol. 2014; 210: S402–3.

45. Lässer C, Eldh M, Lötvall J. Isolation and characterization of RNA-containing exosomes. J Vis Expnet]. 2012: e3037.

46. Bullerdiek J, Flor I. Exosome-delivered microRNAs of "chromosome 19 microRNA cluster" as immunomodulators in pregnancy and tumorigenesis. Mol Cytogenet. 2012; 5: 27. doi: 10.1186/1755-8166-5-27 PMID: 22559272

47. Redman CWG, Sargent IL. Circulating Microparticles in Normal Pregnancy and Pre-Eclampsia. Placenta. 2008; 29: 73–7.

48. Kshirsagar SK, Alam SM, Jasti S, Hodes H, Nauser T, Gilliam M, et al. Immunomodulatory molecules are released from the first trimester and term placenta via exosomes. Placenta. 2012; 33: 982–90. doi: 10.1016/j.placenta.2012.10.005 PMID: 23107341

49. Izumi M, Pazin BJ, Minervini CF, Gerlach J, Ross M a, Stolz DB, et al. Quantitative comparison of stem cell marker-positive cells in fetal and term human amnion. J Reprod Immunol. 2009; 81: 39–43. doi: 10.1016/j.jri.2009.02.007 PMID: 19501410

50. Zhao H, Li Y, Jin H, Xie L, Liu C, Jiang F, et al. Rapid and efficient reprogramming of human amnion-derived cells into pluripotency by three factors OCT4/SOX2/NANOG. Differentiation. 2010; 80: 123–9. doi: 10.1016/j.diff.2010.03.002 PMID: 20510497

51. Koike C, Zhou K, Takeda Y, Fathy M, Okabe M, Yoshida T, et al. Characterization of Amniotic Stem Cells. Cell Reprogram. 2014; 16: 298–305. doi: 10.1089/cell.2013.0090 PMID: 25068631

52. Teng Z, Yoshida T, Okabe M, Toda A, Higuchi O, Nogami M. Establishment of Immortalized Human Amniotic Mesenchymal Stem Cells. Cell Transplant. 2013; 22: 267–78. doi: 10.3727/096368912X655055 PMID: 23006979

53. Gao Y, Pu Y, Wang D, Hou L, Guan W, Ma Y. Isolation and biological characterization of chicken amnion epithelial cells. Eur J Histochem. 2012; 56: e33. doi: 10.4081/ejh.2012.e33 PMID: 23027349

54. Saito S, Lin Y-C, Murayama Y, Hashimoto K, Yokoyama KK. Human amnion-derived cells as a reliable source of stem cells. Curr Mol Med. 2012; 12: 1340–9. PMID: 23016591

55. Andreu Z, Yáñez-Mó M. Tetraspanins in Extracellular Vesicle Formation and Function. Front Immunol. 2014; 5: 1–12.

56. Phimister EG, Phillippe M. Cell-free Fetal DNA—A Trigger for Parturition. N Engl J Med. 2014; 370: 2534–6. doi: 10.1056/NEJMcibr1404324 PMID: 24963574

57. Olivieri F, Albertini MC, Orciani M, Ceka A, Cricca M, Procopio AD, et al. DNA damage response (DDR) and senescence: shuttled inflamma-miRNAs on the stage of inflamm-aging. Oncotarget. 2015; 6: 35509–21. doi: 10.18632/oncotarget.5899 PMID: 26431329

58. Karrasch T, Steinbrecher KA, Allard B, Baldwin AS, Jobin C. Wound-induced p38MAPK-dependent histone H3 phosphorylation correlates with increased COX-2 expression in enterocytes. J Cell Physiol. 2006; 207: 809–15. PMID: 16508963

59. Valbonesi P, Ricci L, Franzellitti S, Biondi C, Fabbri E. Effects of cadmium on MAPK signalling pathways and HSP70 expression in a human trophoblast cell line. Placenta. 2008; 29: 725–33. doi: 10.1016/j.placenta.2008.05.004 PMID: 18571719

60. Behnia F, Sheller S, Menon R. Mechanistic Differences Leading to Infectious and Sterile Inflammation. Am J Reprod Immunol. 2016; 75: 505–18. doi: 10.1111/aji.12496 PMID: 26840942

61. Derynck R, Muthusamy BP, Saeteurn KY. Signaling pathway cooperation in TGF-β-induced epithelial-mesenchymal transition. Curr Opin Cell Biol. 2014; 31: 56–66. doi: 10.1016/j.ceb.2014.09.001 PMID: 25240174

62. Papageorgis P. TGFβ Signaling in Tumor Initiation, Epithelial-to-Mesenchymal Transition, and Metastasis. J Oncol. 2015; 2015: 587193. doi: 10.1155/2015/587193 PMID: 25883652

63. Fabregat I, Malfettone A, Soukupova J. New Insights into the Crossroads between EMT and Stemness in the Context of Cancer. J Clin Med. 2016;5.

64. Da C, Liu Y, Zhan Y, Liu K, Wang R. Nobiletin inhibits epithelial-mesenchymal transition of human non-small cell lung cancer cells by antagonizing the TGF-β1/Smad3 signaling pathway. Oncol Rep. 2016; 35: 2767–74. doi: 10.3892/or.2016.4661 PMID: 26986176

65. Yeh Y-H, Wang S-W, Yeh Y-C, Hsiao H-F, Li T-K. Rhapontigenin inhibits TGF-β-mediated epithelial-mesenchymal transition via the PI3K/AKT/mTOR pathway and is not associated with HIF-1α degradation. Oncol Rep. 20169; 35: 2887–95. doi: 10.3892/or.2016.4664 PMID: 26986649

66. Romero R, Kusanovic JP, Gomez R, Lamont R, Bytautiene E, Garfield RE, et al. The clinical significance of eosinophils in the amniotic fluid in preterm labor. J Matern Fetal Neonatal Med. 2010; 23: 320–9. doi: 10.3109/14767050903168465 PMID: 19900034

67. Menon R, Fortunato SJ, Milne GL, Brou L, Carnevale C, Sanchez SC, et al. Amniotic fluid eicosanoids in preterm and term births: effects of risk factors for spontaneous preterm labor. Obstet Gynecol. 2011; 118: 121–34. doi: 10.1097/AOG.0b013e3182204eaa PMID: 21691170

68. Menon R. Oxidative stress damage as a detrimental factor in preterm birth pathology. Front Immunol. 2014; 5: 567. doi: 10.3389/fimmu.2014.00567 PMID: 25429290

69. Harding C V., Heuser JE, Stahl PD. Exosomes: Looking back three decades and into the future. J Cell Biol. 2013; 200: 367–71. doi: 10.1083/jcb.201212113 PMID: 23420870

70. György B, Szabó TG, Pásztói M, Pál Z, Misják P, Aradi B, et al. Membrane vesicles, current state-of-the-art: Emerging role of extracellular vesicles. Cell Mol Life Sci. 2011; 68: 2667–88. doi: 10.1007/s00018-011-0689-3 PMID: 21560073

71. Hornung D, Lebovic DI, Shifren JL, Vigne JL, Taylor RN. Vectorial secretion of vascular endothelial growth factor by polarized human endometrial epithelial cells. Fertil Steril. 1998; 69: 909–15. PMID: 9591502

72. Mesiano S, Chan EC, Fitter JT, Kwek K, Yeo G, Smith R. Progesterone withdrawal and estrogen activation in human parturition are coordinated by progesterone receptor A expression in the myometrium. J Clin Endocrinol Metab. 2002; 87: 2924–30. PMID: 12050275

73. Merlino A a., Welsh TN, Tan H, Li JY, Cannon V, Mercer BM, et al. Nuclear progesterone receptors in the human pregnancy myometrium: Evidence that parturition involves functional progesterone withdrawal mediated by increased expression of progesterone receptor-A. J Clin Endocrinol Metab. 2007; 92(5): 1927–33. PMID: 17341556

74. Mesiano S. Myometrial progesterone responsiveness. Semin Reprod Med. 2007; 25: 5–13. PMID: 17205419

75. Mesiano S, Wang Y, Norwitz ER. Progesterone receptors in the human pregnancy uterus: do they hold the key to birth timing? Reprod Sci. 2011; 18: 6–19. doi: 10.1177/1933719110382922 PMID: 20889955

76. Dressing GE, Knutson TP, Schiewer MJ, Daniel AR, Hagan CR, Diep CH, et al. Progesterone receptor-cyclin D1 complexes induce cell cycle-dependent transcriptional programs in breast cancer cells. Mol Endocrinol. 2014; 28: 442–57. doi: 10.1210/me.2013-1196 PMID: 24606123

77. Beck C a., Zhang Y, Altmann M, Weigel NL, Edwards DP. Stoichiometry and Site-specific Phosphorylation of Human Progesterone Receptor in Native Target Cells and in the Baculovirus Expression System. J Biol Chem. 1996; 271(32): 19546–55. PMID: 8702648

78. Beck CA, Zhang Y, Weigel NL, Edwards DP. Two Types of Anti-progestins Have Distinct Effects on Site-specific Phosphorylation of Human Progesterone Receptor. J Biol Chem. 1996; 271: 1209–17. PMID: 8557652

79. Zhang Y, Beck CA, Poletti A, Edwards DP, Weigel NL. Identification of a group of Ser-Pro motif hormone-inducible phosphorylation sites in the human progesterone receptor. Mol Endocrinol. 1995; 9: 1029–40. PMID: 7476977

80. Delorme-Axford E, Bayer A, Sadovsky Y, Coyne CB. Autophagy as a mechanism of antiviral defense at the maternal-fetal interface. Autophagy. 2013; 9: 2173–4. doi: 10.4161/auto.26558 PMID: 24231730

81. Li JYZ, Yong TY, Michael MZ, Gleadle JM. MicroRNAs: are they the missing link between hypoxia and pre-eclampsia? Hypertens pregnancy. 2014; 33: 102–14. doi: 10.3109/10641955.2013.832772 PMID: 24354525

82. Vargas A, Zhou S, Ethier-Chiasson M, Flipo D, Lafond J, Gilbert C, et al. Syncytin proteins incorporated in placenta exosomes are important for cell uptake and show variation in abundance in serum exosomes from patients with preeclampsia. FASEB J. 2014; 28: 3703–19. doi: 10.1096/fj.13-239053 PMID: 24812088

83. Kambe S, Yoshitake H, Yuge K, Ishida Y, Ali MM, Takizawa T, et al. Human exosomal placenta-associated miR-517a-3p modulates the expression of PRKG1 mRNA in Jurkat cells. Biol Reprod. 2014; 91: 129. doi: 10.1095/biolreprod.114.121616 PMID: 25273530

84. Mincheva-Nilsson L, Baranov V. The Role of Placental Exosomes in Reproduction. Am J Reprod Immunol. 2010; 63: 520–33. doi: 10.1111/j.1600-0897.2010.00822.x PMID: 20331583

85. Mincheva-Nilsson L, Baranov V. Placenta-Derived Exosomes and Syncytiotrophoblast Microparticles and their Role in Human Reproduction: Immune Modulation for Pregnancy Success. Am J Reprod Immunol. 2014; 72: 440–57. doi: 10.1111/aji.12311 PMID: 25164206

86. Record M. Intercellular communication by exosomes in placenta: A possible role in cell fusion? Placenta. 2014; 35: 297–302. doi: 10.1016/j.placenta.2014.02.009 PMID: 24661568

87. Stenqvist A-C, Nagaeva O, Baranov V, Mincheva-Nilsson L. Exosomes secreted by human placenta carry functional Fas ligand and TRAIL molecules and convey apoptosis in activated immune cells, suggesting exosome-mediated immune privilege of the fetus. J Immunol. 2013; 191: 5515–23. doi: 10.4049/jimmunol.1301885 PMID: 24184557

88. Southcombe J, Tannetta D, Redman C, Sargent I. The immunomodulatory role of syncytiotrophoblast microvesicles. PLoS One. 2011; 6: e20245. doi: 10.1371/journal.pone.0020245 PMID: 21633494

89. Atay S, Gercel-Taylor C, Kesimer M, Taylor DD. Morphologic and proteomic characterization of exosomes released by cultured extravillous trophoblast cells. Exp Cell Res. 2011; 317: 1192–202. doi: 10.1016/j.yexcr.2011.01.014 PMID: 21276792

90. Atay S, Gercel-Taylor C, Suttles J, Mor G, Taylor DD. Trophoblast-derived exosomes mediate monocyte recruitment and differentiation. Am J Reprod Immunol. 2011; 65: 65–77. doi: 10.1111/j.1600-0897.2010.00880.x PMID: 20560914

91. Atay S, Gercel-Taylor C, Taylor DD. Human trophoblast-derived exosomal fibronectin induces pro-inflammatory IL-1β production by macrophages. Am J Reprod Immunol. 2011; 66: 259–69. doi: 10.1111/j.1600-0897.2011.00995.x PMID: 21410811

92. Redman CWG, Tannetta DS, Dragovic R a, Gardiner C, Southcombe JH, Collett GP, et al. Review: Does size matter? Placental debris and the pathophysiology of pre-eclampsia. Placenta. 2012; 33: S48–54. doi: 10.1016/j.placenta.2011.12.006 PMID: 22217911

93. Salomon C, Yee SW, Mitchell MD, Rice GE. The Possible Role of Extravillous Trophoblast-Derived Exosomes on the Uterine Spiral Arterial Remodeling under Both Normal and Pathological Conditions. Biomed Res Int. 2014; 2014: 1–10.

94. Kobayashi M, Salomon C, Tapia J, Illanes SE, Mitchell MD, Rice GE. Ovarian cancer cell invasiveness is associated with discordant exosomal sequestration of Let-7 miRNA and miR-200. J Transl Med. 2014; 12: 4. doi: 10.1186/1479-5876-12-4 PMID: 24393345